

SCAMP5 regulates AP-4-dependent sorting and trafficking of ATG9A for presynaptic autophagy via PI4KB/PI4KIII β recruitment and PtdInsP4 production at the TGN

Seung Hyun Ryu , Jungmihn Lee , Unghwi Lee , Kitae Kim , Go-Eun Jun , Jeongmin Oh , Sang-Eun Lee & Sunghoe Chang

To cite this article: Seung Hyun Ryu , Jungmihn Lee , Unghwi Lee , Kitae Kim , Go-Eun Jun , Jeongmin Oh , Sang-Eun Lee & Sunghoe Chang (16 Sep 2025): SCAMP5 regulates AP-4-dependent sorting and trafficking of ATG9A for presynaptic autophagy via PI4KB/PI4KIII β recruitment and PtdInsP4 production at the TGN, Autophagy, DOI: [10.1080/15548627.2025.2559689](https://doi.org/10.1080/15548627.2025.2559689)

To link to this article: <https://doi.org/10.1080/15548627.2025.2559689>



[View supplementary material](#)



Published online: 16 Sep 2025.



[Submit your article to this journal](#)



Article views: 201



[View related articles](#)



[View Crossmark data](#)

RESEARCH PAPER



SCAMP5 regulates AP-4-dependent sorting and trafficking of ATG9A for presynaptic autophagy via PI4KB/PI4KIII β recruitment and PtdInsP4 production at the TGN

Seung Hyun Ryu^{a,b}, Jungmihn Lee^{a*}, Unghwi Lee^{a,c}, Kitae Kim^a, Go-Eun Jun^a, Jeongmin Oh^a, Sang-Eun Lee^{a,d}, and Sunghoe Chang ^{a,b}

^aDepartment of Physiology and Biomedical Sciences, Seoul National University College of Medicine, Seoul, South Korea; ^bInterdisciplinary Program in Neuroscience, Seoul National University, Seoul, South Korea; ^cDepartment of Biochemistry and Biophysics, Kavli Institute for Fundamental Neuroscience, University of California, San Francisco, CA, USA; ^dDepartment of Life Sciences, CHA University, Seongnam-si, Gyeonggi-do, South Korea

ABSTRACT

Neuronal autophagosome formation at distant presynaptic sites relies on ATG9A trafficking, a process mediated by AP-4 at the trans-Golgi network (TGN), but the molecular mechanisms governing its sorting for presynaptic delivery have remained elusive. Here, we uncover an unexpected role for SCAMP5, a key regulator of synaptic vesicle dynamics, in orchestrating presynaptic macroautophagy/autophagy through its actions at the TGN. SCAMP5 depletion severely impairs autophagosome formation at presynaptic boutons. Mechanistically, we identify SCAMP5 as a novel binding partner of PI4KB/PI4KIII β (phosphatidylinositol 4-kinase beta), where it controls PI4KB recruitment to the TGN and subsequent phosphatidylinositol-4-phosphate (PtdIns4P) production. As PtdIns4P is essential for AP-4 recruitment, SCAMP5 depletion disrupts AP-4-mediated ATG9A trafficking to presynaptic sites, thereby compromising presynaptic autophagy and subsequent protein turnover. Our findings establish that SCAMP5 coordinates ATG9A-dependent presynaptic autophagy through PI4KB recruitment and PtdIns4P production at the TGN, revealing a novel pathway critical for maintaining presynaptic protein homeostasis.

Abbreviations: AP-4: adaptor protein 4; ATG9A: autophagy related 9A; PI4KB/PI4KIII β : phosphatidylinositol 4-kinase beta; PtdIns4P: phosphatidylinositol-4-phosphate; SCAMP5: secretory carrier membrane protein 5; TGN: trans-Golgi network.

ARTICLE HISTORY

Received 10 February 2025

Revised 23 August 2025

Accepted 8 September 2025

KEYWORDS

AP-4; ATG9A; PI4KB/PI4KIII β ; presynaptic autophagy; SCAMP5

Introduction

Macroautophagy (hereafter called autophagy), is a protein-degradative pathway vital for cellular homeostasis, growth, differentiation, and development [1–4]. ATG (autophagy related) proteins serve as critical markers for the identifying and characterizing of each step in the autophagy process [5]. Among these, ATG9A stands out as the only transmembrane protein, playing a vital role in initiating phagophore formation. In neurons, autophagy is a constitutively active process both at rest and during activity, by effectively eliminating dysfunctional organelles and damaged proteins from distal presynaptic terminals [6–8].

Proper cargo sorting and trafficking rely on the recruitment of specific adaptor protein (AP) complexes (AP-1, 2, 3, 4, or 5) to the trans-Golgi network (TGN). AP-4, for instance, associates with the TGN via direct interaction with ARF1 in its GTP-bound state, a process facilitated by AP4E1 and AP4M1 subunits [9]. ARF1, a small GTPase, is essential for the recruitment of the AP-4 complex to the TGN and ARF1 activation facilitates the binding of AP-4 to the Golgi membranes, thereby promoting cargo sorting and vesicle formation [9]. Phosphatidylinositol-4-

phosphate (PtdIns4P) is essential for the recruitment of ARF1 to the TGN [10]. Therefore, the interaction between PtdIns4P and ARF1 ensures the proper localization and function of AP-4 at the TGN, which is crucial for vesicle formation and trafficking [11,12]. Several proposed AP-4 cargos include APP (amyloid beta precursor protein), APLP1 (amyloid beta precursor like protein 1) and APLP2 [13,14], NAGPA (N-acetylglucosamine-1-phosphodiester alpha-N-acetylglucosaminidase) [15], ATG9A (autophagy related 9A) [16], and SERINC1 (serine incorporator 1) and SERINC3 [17]. AP-4 mediates the basolateral sorting of cargos in epithelial cells [18,19] and the distribution of some dendritic proteins, such as GRID2 (glutamate ionotropic receptor delta type subunit 2) [20] and CACNG2/TARP γ -2/stargazin (calcium voltage-gated channel auxiliary subunit gamma 2), is also thought to depend on AP-4 [21].

PtdIns4P is a key lipid for the identity of the TGN. PtdIns4P is generated from phosphatidylinositol by phosphatidylinositol 4-kinases (PI4Ks). Mammalian cells express at least three Golgi-membrane-localized PI4Ks – PI4K2A/PI4KII α , PI4KA/

CONTACT Sang-Eun Lee sangeun@cha.ac.kr Department of Life Sciences, #616, 335 Pangyo-ro Bundang-gu, Seongnam-si, Gyeonggi-do 13496, South Korea; Sunghoe Chang sunghoe@snu.ac.kr Department of Physiology and Biomedical Sciences, Seoul National University College of Medicine, #309 Medical Science Building, 103 Daehak-ro Jongno-gu, Seoul 03080, South Korea

*These authors contributed equally.

This article has been republished with minor changes. These changes do not impact the academic content of the article.

Supplemental data for this article can be accessed online at <https://doi.org/10.1080/15548627.2025.2559689>

PI4KIII α , and PI4KB/PI4KIII β , of which PI4K2A and PI4KB have been implicated in Golgi-complex-to-cell-surface transport [22–24]. PI4KA achieves stable membrane association through palmitoylation, while PI4KB recruitment relies on protein-protein interactions, such as those with ACBD3 (acyl-CoA binding domain containing 3) [25] or GGAs (golgi associated, gamma adaptin ear containing, ARF binding protein) [26]. However, the precise molecular mechanism of PI4KB recruitment to the Golgi is still poorly understood.

Neurons face unique challenges in regulating autophagy due to their post-mitotic state, distinctive morphology, and specialized metabolic requirements [27,28]. Studies in *C. elegans* have revealed that autophagosome formation occurs preferentially near synaptic sites within axons, facilitated by UNC-104/KIF1A-mediated transport of ATG-9 [29]. Research has shown that the ubiquitin ligase RPM-1/MYCBP2 modulates autophagy by constraining the activity of UNC-51/ULK kinase, a key autophagy initiator, within specific axonal domains [30]. Furthermore, recent work has identified the active zone protein CLA-1/SCARB1 as an essential mediator of ATG-9 sorting at synapses through endosome-dependent endocytosis, thereby controlling activity-dependent presynaptic autophagy [31]. Additionally, emerging evidence has revealed novel roles for classical endocytic proteins – including SH3GL family/endophilin, SYNJ1 (synaptjanin 1), and BSN/bassoon – in both the genesis and trafficking of autophagosomes at presynaptic terminals [32–34].

ATG9A has been identified as a specific AP-4 cargo, with AP-4 facilitating ATG9A export from the TGN to support peripheral autophagosome formation [16]. Mutations in AP-4 subunits cause AP-4 deficiency syndrome (AP-4-associated HSP), where neuroaxonal dystrophy stems from disrupted ATG9A distribution and axonal aggregate formation [35–38]. ATG9A localizes to presynaptic terminals via AP-4-mediated transport [16,39], undergoing activity-dependent exo-endocytosis to regulate presynaptic autophagy [40]. Recent evidence indicates that ATG9A-containing vesicles concentrate at presynaptic terminals as a distinct population from synaptic vesicles [41], with ATG9A distributed across somatic TGN, dendrites, axons, and presynaptic regions [42,43]. The substantial spatial separation between neuronal soma and presynaptic terminals demands sophisticated ATG9A trafficking mechanisms. While research has established ATG9A's role in distal autophagosome formation and subsequent retrograde trafficking for somatic degradation, the molecular determinants governing ATG9A sorting at the TGN and its anterograde axonal transport remain poorly understood.

SCAMPs (secretory carrier membrane protein), a family of ubiquitous tetra-spanning vesicle membrane proteins, are known to function in vesicular trafficking and recycling processes. Previous studies suggested that different SCAMPs may mark different pathways at TGN and endosomal compartments depending on their preferential interactions with adaptor proteins [44,45]. Among five SCAMPs (SCAMP1 to

SCAMP5), SCAMP1 and SCAMP5 are highly expressed in the brain and synaptic vesicle (SV) [44]. Recent research has highlighted the significance of SCAMP5 deficiency in the pathogenesis of various neurodevelopmental diseases such as autism, pediatric epilepsy, and Parkinson disease [46–48]. We previously showed the critical role of SCAMP5 in SV endocytosis during high neuronal activity conditions [49], regulating short-term depression through release site clearance [50], and axonal trafficking and synaptic localization of SLC9A6/NHE6 to modulate quantal size [51]. Besides in synaptic vesicles, SCAMP5 is also highly enriched at the TGN, yet its functional significance remains uninvestigated.

In this study, we found that SCAMP5 deficiency impaired autophagosome formation in presynaptic boutons, revealing its critical role in presynaptic autophagy. Further investigation revealed that SCAMP5 interacts with PI4KB, and SCAMP5 knockdown (KD) disrupts PI4KB recruitment, leading to impaired localized production of PtdIns4P and a significant decrease in PtdIns4P levels at the TGN. Since the localized production of PtdIns4P is necessary for the recruitment of ARF1 and AP-4, SCAMP5 KD impairs AP-4 and ARF1 recruitment at the TGN, hindering the export of ATG9A and leading to its accumulation there. This effect mirrors that observed upon knockout of genes encoding AP-4 components. Consequently, SCAMP5 KD results in the impediment of ATG9A axonal trafficking, subsequently impairing presynaptic autophagy and causing the accumulation of an older pool of synaptic vesicle proteins. While significant progress has been made in understanding the molecular machinery of presynaptic autophagy, our study elucidates the underlying mechanism of how ATG9A is sorted and exported at the TGN, which is essential for proper autophagy and maintaining protein homeostasis at synapses. Our findings highlight SCAMP5 as a critical regulator in these processes.

Results

SCAMP5 is highly enriched at the Golgi network and its depletion caused defects in the presynaptic autophagosome formation

SCAMPs are distributed across secretion granules, transporter vesicles, endosomal compartments, and Golgi membranes [51–55]. To investigate the subcellular distribution of SCAMP5, we first performed immunocytochemistry using antibodies against EEA1, LAMP1, GOLGB1/Giantin, and TGOLN2/TGN38 together with SCAMP5 in the primary rat hippocampal neurons (Figure 1A,B and Figure S1A-B). Consistent with previous results [51,56], SCAMP5 was significantly enriched at presynaptic boutons, colocalizing with SYP (synaptophysin) (Figure 1A,B). Interestingly, we also found that high abundance of SCAMP5 at the Golgi network, colocalizing with cis-medial Golgi marker GOLGB1 and trans-Golgi marker TGOLN2 but not with early endosome marker EEA1 or lysosome marker LAMP1 (Figures S1A and B). This notable enrichment in the Golgi network is not

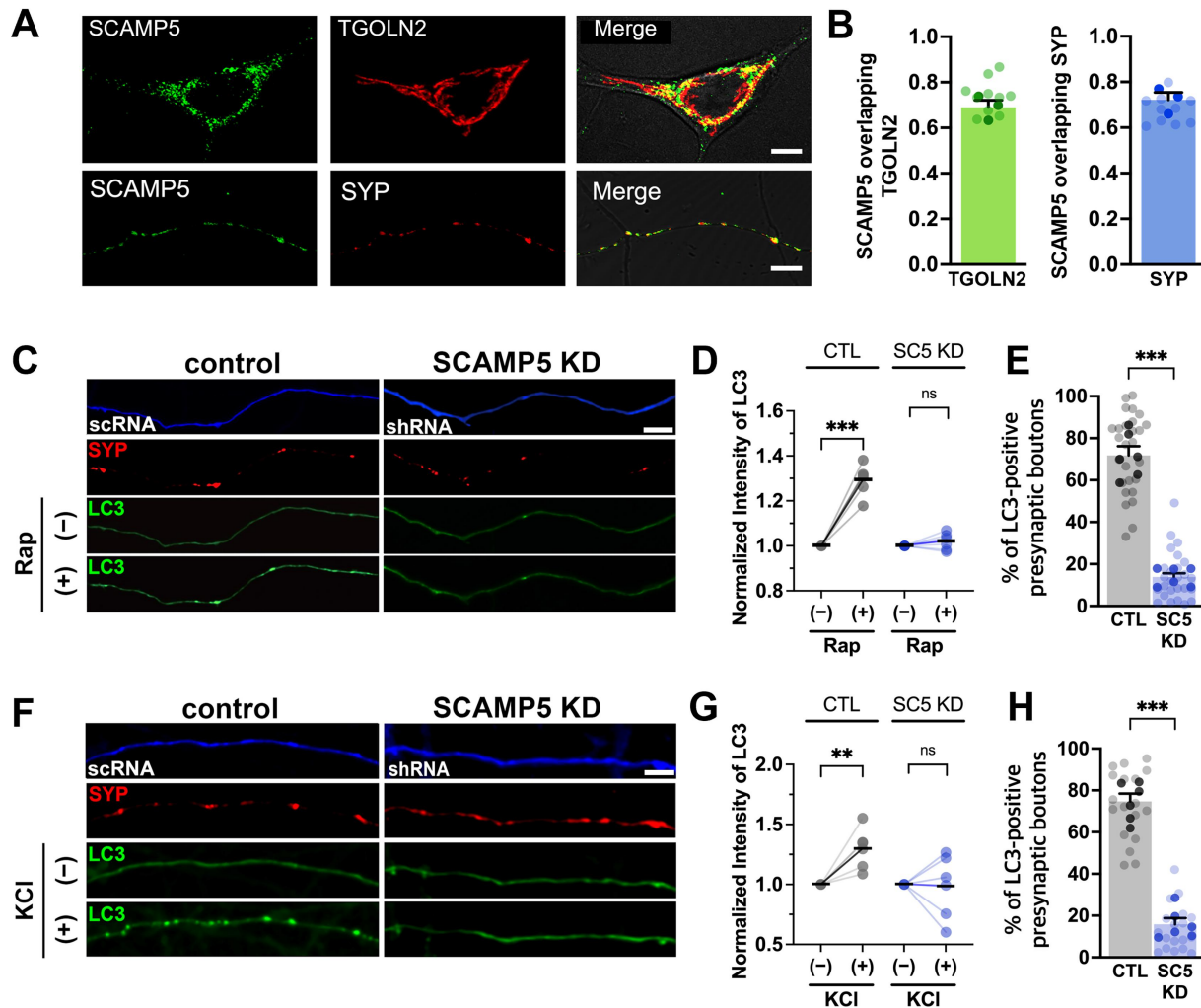


Figure 1. SCAMP5 is highly enriched at the trans-Golgi network and its depletion caused defects in the presynaptic autophagosome formation. (A) Rat hippocampal neurons were immunostained with specific antibodies to detect endogenous localization of SCAMP5, TGOLN2/TGN38 (TGN marker), or SYP. Scale bar: 5 μm. (B) Mander's colocalization coefficients showing SCAMP5 overlap with TGOLN2 in the soma (0.69 ± 0.032 , $n = 3$, left) and with SYP in the presynaptic terminals (0.72 ± 0.031 , $n = 3$, right). (C and F) Representative images of cultured rat hippocampal neurons co-transfected with mTagbfp2-scRNA (sequence-scrambled shRNA) or shRNA of *Scamp5* (blue), mCherry-SYP (red), and EGFP-LC3 (green) with or without treatment of rapamycin (C) or high KCl (F) for autophagy induction. Scale bar: 5 μm. (D) Quantification of the normalized relative intensity of EGFP-LC3 expression in control (CTL) and SCAMP5 KD neurons (SC5 KD) with or without treatment of rapamycin. CTL: 1.29 ± 0.028 , $n = 6$ (102 boutons); $p < 0.001$, SC5 KD: 1.02 ± 0.015 , $n = 6$ (102 boutons); $p = 0.245$, analyzed by Student's t-test. (E) Percentage of LC3-positive presynaptic boutons in control and SCAMP5 KD neurons after rapamycin treatment, CTL: 71.80 ± 4.352 , $n = 6$ (27 axons); SC5 KD: 13.85 ± 1.811 , $n = 6$ (26 axons); $p < 0.001$, analyzed by Student's t-test. Values are indicated as mean \pm SEM. (G) Quantification of the normalized relative intensity of EGFP-LC3 expression in CTL and SCAMP5 KD neurons with or without treatment of high KCl. CTL: 1.30 ± 0.067 , $n = 6$ (104 boutons); $p = 0.001$, analyzed by Student's t-test, SCAMP5 KD: 0.98 ± 0.107 , $n = 6$ (104 boutons); $p = 0.8742$, analyzed by Student's t-test. (H) Percentage of LC3-positive presynaptic boutons in control and SCAMP5 KD neurons after high KCl treatment, CTL: 74.71 ± 3.736 , $n = 6$ (18 axons); SC5 KD: 15.83 ± 2.951 , $n = 6$ (18 axons); $p = 0.0226$, analyzed by Student's t-test. Each shaded point represents data from a single neuron, and each filled point represents the mean of each independent experiment. Values are indicated as mean \pm SEM. ** $p < 0.01$, *** $p < 0.001$, ns: not significant.

observed with SYP, suggesting a selective role of SCAMP5 at the Golgi network (Figures S1C and D).

Although the link between SCAMP5 and autophagy has previously been suggested particularly when cells are under stress conditions like protein or ER stress [57,58], no definitive role for SCAMP5 in autophagy has been demonstrated. When we downregulated the expression of endogenous SCAMP5 using a small hairpin RNA (shRNA) [49–51] and induced autophagy by the treatment with rapamycin, a well-established autophagy inducer in neuronal cells [59], we observed unexpected differential effects on autophagosome formation (Figures S2C and D). While basal levels of LC3-positive autophagosomes were

comparable between control and SCAMP5 knockdown (KD) neurons (Figure S2A), rapamycin treatment revealed a striking difference, with SCAMP5 KD neurons showing markedly reduced LC3-positive autophagosome formation at presynaptic boutons, whereas control neurons exhibited increased autophagosome formation at these sites in hippocampal cultures (Figure 1C–E).

These findings were further corroborated using 90 mM KCl to induce activity-dependent autophagy in neurons [60]. Again, basal presynaptic autophagosome formation was comparable between control and SCAMP5 KD neurons and high KCl treatment failed to significantly induce presynaptic autophagosome formation in SCAMP5 KD

neurons compared to controls (Figure 1G–J and Figure S2B). These results suggest that SCAMP5 plays a role in regulating autophagosome formation, particularly at presynaptic boutons.

SCAMP5 interacts with PI4KB, which is essential for PI4KB localization and subsequent PtdIns4P production at the TGN

Recent studies show that AP-4 exports the autophagy protein ATG9A from the TGN and promotes early autophagosome formation [16,61]. The recruitment of ARF1 and AP-1 or AP-4 at the TGN is regulated by PtdIns4P production through PI4Ks [9,62,63]. We also found that, upon rapamycin treatment, the synthesis of ATG9A and ARF1 increased (Figures S2E and F).

PI4KB recruitment to the TGN is known to depend on interactions with GGAs [26] or ACBD3 [25], though the exact mechanism remains unclear. The binding between ACBD3 and PI4KB relies on a short helical region of ACBD3 rich in glutamine residues (Q domain) and the N-terminal region of PI4KB [64]. We found that the C-terminal region of SCAMP5 contains multiple glutamine residues and the AlphaFold3 predictions suggest potential binding interactions between the glutamine-rich helical region of SCAMP5 C-terminal region and the N-terminal helical region of PI4KB (Figure 2A and Figure S3A).

To test this possibility, we co-transfected HEK-293T cells with EGFP-tagged full-length SCAMP5 or the C-terminal region containing the fourth transmembrane region (TM4-Ct) of SCAMP5 and FLAG-tagged PI4KB, followed by a co-immunoprecipitation assay. We found that both the full-length SCAMP5 and the TM4-Ct of SCAMP5 interact with PI4KB (Figure 2B). Additionally, we demonstrated the direct interaction between the SCAMP5 C-terminal region and PI4KB by *in vitro* binding assay using purified proteins (Figure 2C).

To investigate whether interaction with SCAMP5 is necessary for the recruitment of PI4KB to the TGN, we immunostained PI4KB together with TGOLN2 in control and SCAMP5 KD neurons. We first validated the specificity of the PI4KB antibody using western blotting in HEK-293T cells and immunostaining in HeLa cells after siRNA-mediated knockdown (Figures S4C–F). We then assessed PI4KB distribution at the TGN using this validated antibody and observed a significant reduction in PI4KB immunoreactivity at the TGN in SCAMP5 KD neurons compared to control neurons (Figure 2D–F). Decreased recruitment of PI4KB implies defects in PtdIns4P production at the TGN in SCAMP5 KD neurons. Using the established PtdIns4P probe EGFP-PH^{FAPP1} [65], we confirmed the predominant TGN localization for PtdIns4P in control neurons but found a significant reduction in PtdIns4P levels at the TGN of SCAMP5 KD neurons compared to control neurons (Figure 2G,H). Additionally, the total levels of PI4KB were comparable between control and SCAMP5 KD neurons (Figures S4A and B). These findings suggest a model in which the interaction with SCAMP5

is critical for the recruitment of PI4KB and the production of PtdIns4P at the TGN in the soma.

SCAMP5 KD causes the defects in AP-4 and ARF1 recruitments at the TGN in neurons

The previous findings that PtdIns4P production by PI4Ks is essential for recruiting ARF1 and AP-4 at the TGN [9,62,63] suggest defects in ARF1 and AP-4 recruitment in SCAMP5 KD neurons.

To test this possibility, we used an AP4E1 antibody to assess overall AP-4 localization. We observed significant colocalization of AP-4 and TGOLN2 in control neurons, which was markedly reduced in SCAMP5 KD neurons (Figure 3A–C and Figure S4G). We further showed that even with AP4M1 overexpression, AP4M1 localization at the TGN was significantly reduced in SCAMP5 KD neurons (Figures S5A and B).

Additionally, we examined the localization of ARF1. As expected, ARF1 colocalized extensively with the TGOLN2 in control neurons, but this colocalization was significantly diminished in SCAMP5 KD neurons (Figure 3D–F). We further showed that although overall levels of ARF1 were increased in SCAMP5 KD neurons (Figures S6A and B), ARF1 was dispersed along neighboring neurites rather than being properly localized at the TGN (Figures S6C and D). This result is in stark contrast to that observed with rapamycin treatment, where both total ARF1 levels and TGN localization were significantly increased (Figures S2E–K).

These results suggest that the interaction between SCAMP5 and PI4KB plays a critical role in ensuring proper ARF1-mediated AP-4 localization at the TGN, potentially influencing its function in cargo trafficking and autophagy.

SCAMP5 also interacts with AP-4 via its N-terminal region

Different SCAMP proteins exhibit distinct interacting patterns, with SCAMP2 interacting with AP-1 and SCAMP3 with AP-3 [45]. Interestingly, our previous work identified SCAMP5 interacting with AP-2 at presynaptic terminals [50]. It raises the possibility that SCAMP5 interacts with an AP complex at the TGN.

To identify the interaction between SCAMP5 and adapter proteins, we performed a co-immunoprecipitation assay and found that SCAMP5 interacts with AP-4 (AP4M1) as well as with AP-2 (AP2M1) as previously found, but not with AP-1 (AP1M1) in the rat hippocampal neurons (Figure 4A–C). When immunostained, SCAMP5 showed high colocalization with AP-4 at the TGN within the cell body of cultured neurons (Figure 4D,E).

We next sought to delineate the AP-4 binding domain of SCAMP5 (Figure 4F–I). While the full length of SCAMP5 binds to AP4M1, none of the cytosolic domains of SCAMP5 (Nt cyto, 2/3 cyto, and Ct cyto) interacted with AP4M1 (Figure 4G). However, the N-terminal region containing the first transmembrane region (Nt-TM1) of SCAMP5 bound to AP4M1, while the C-terminal region containing the fourth transmembrane region (TM4-Ct) and 2/3 loop flanked by a transmembrane region at

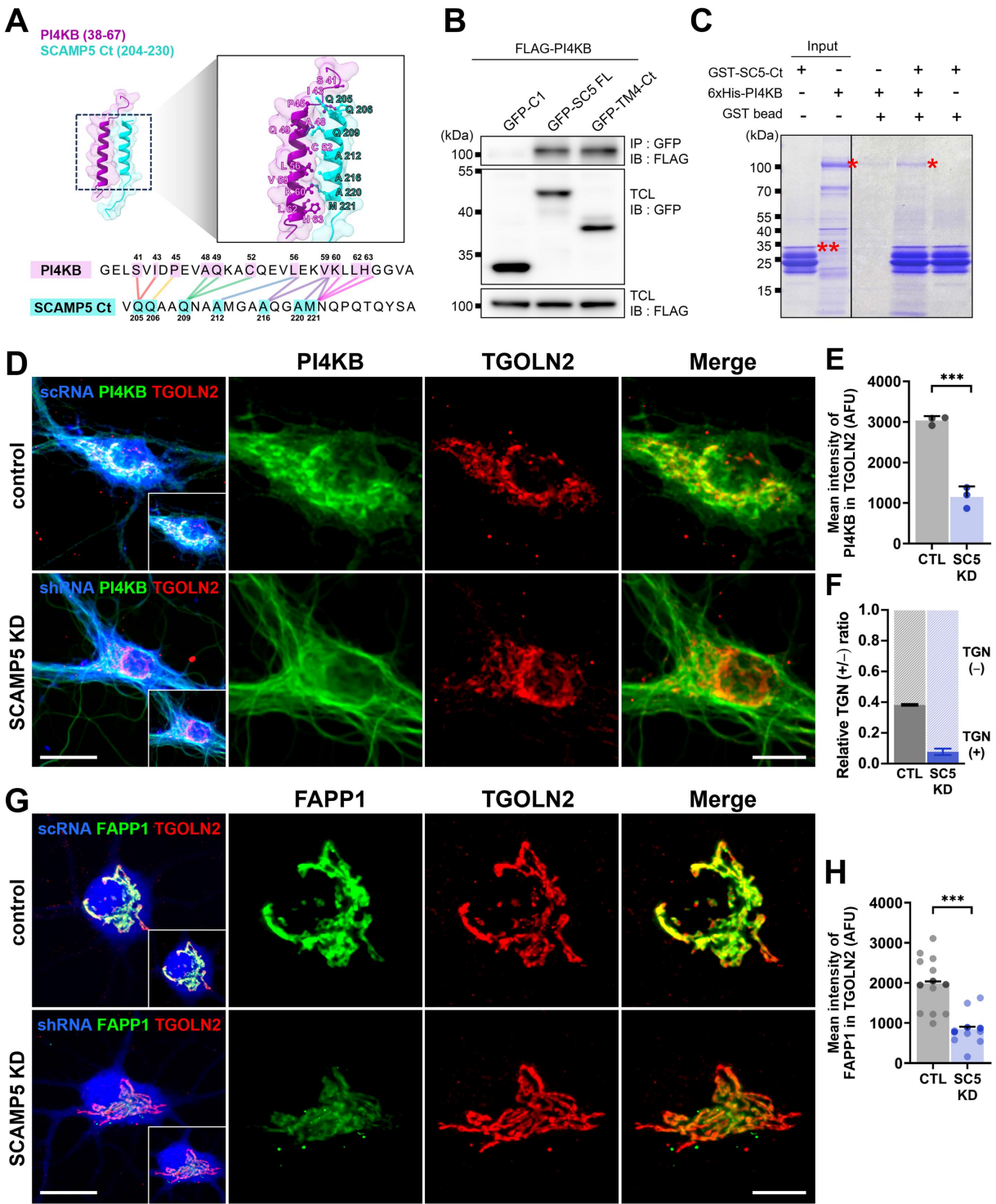


Figure 2. SCAMP5 interacts with PI4KB, which is essential for PI4KB localization and subsequent PtdIns4P production at the TGN. (A) Alphafold3-predicted putative contact sites (residues with center-to-center atomic distance $\leq 4 \text{ \AA}$) between the C-terminal Q-rich helical region of SCAMP5 (residue 204–230, cyan) and PI4KB N-terminal helical region (residue 38–67, magenta). The overall pTM and iPTM scores were 0.64 and 0.56 but the SCAMP5's interaction with PI4KB is predicted confidently (pLLDT confidence measure > 90) as judged by the corresponding parts of the PAE plot (see Figure S3A). (B) FLAG-tagged PI4KB and EGFP-tagged SCAMP5 full-length (FL) or C-terminal region containing the fourth transmembrane domain (residues 194–235; TM4-Ct) were co-expressed in HEK-293T cells, followed by cell lysis and co-immunoprecipitation using anti-GFP antibody, and detection of immunoprecipitated proteins with anti-FLAG antibody. IP: immunoprecipitation; IB: immunoblotting; TCL: total cell lysates. (C) 6xHis-PI4KB and GST-SCAMP5-Ct were purified, mixed, and incubated with Glutathione Agarose resin, followed by SDS-PAGE analysis. *: PI4KB, **: SCAMP5-Ct. (D) Representative images of cultured rat hippocampal neurons transfected with scRNA or shRNA for SCAMP5 KD (SC5 KD), followed by immunostaining with anti-PI4KB and anti-TGOLN2/TGN38 antibodies. Scale bar: 25 μm ; 5 μm . (E) Mean intensity of PI4KB immunoreactivity at the TGN (outlined based on the TGOLN2 staining pattern in the merged panel) in control or SCAMP5 KD neurons. CTL: 3035.54 ± 61.556 , $n = 3$ (10 neurons); SC5 KD: 1149.39 ± 150.313 , $n = 3$ (10 neurons); $p < 0.001$, analyzed by Student's *t*-test. AFU, arbitrary fluorescence units. Values are indicated as mean \pm SEM. (F) The relative ratio of PI4KB in TGN-positive versus TGN-negative regions of control and SCAMP5 KD neurons, CTL: 0.38 ± 0.006 , $n = 3$ (11 neurons); SC5 KD: 0.08 ± 0.028 , $n = 3$ (11 neurons). Values are indicated as mean \pm SEM. (G) Representative images of cultured rat hippocampal neurons transfected with scRNA or shRNA of SCAMP5 KD and EGFP-PH^{FAPP1} (PtdIns4P probe, FAPP1), followed by immunostaining with anti-TGOLN2/TGN38 antibody. Scale bar: 25 μm ; 5 μm . (H) Mean intensity of EGFP-PH^{FAPP1} at the TGN (outlined based on the TGOLN2 staining pattern in the merged panel) in control or SCAMP5 KD neurons. CTL: 1984.33 ± 30.368 , $n = 3$ (10 neurons); SC5 KD: 846.09 ± 34.793 , $n = 3$ (9 neurons); $p < 0.001$, analyzed by Student's *t*-test. Each shaded point represents data from a single neuron, and each filled point represents the mean of each independent experiment. AFU, arbitrary fluorescence units. Values are indicated as mean \pm SEM. *** $p < 0.001$.

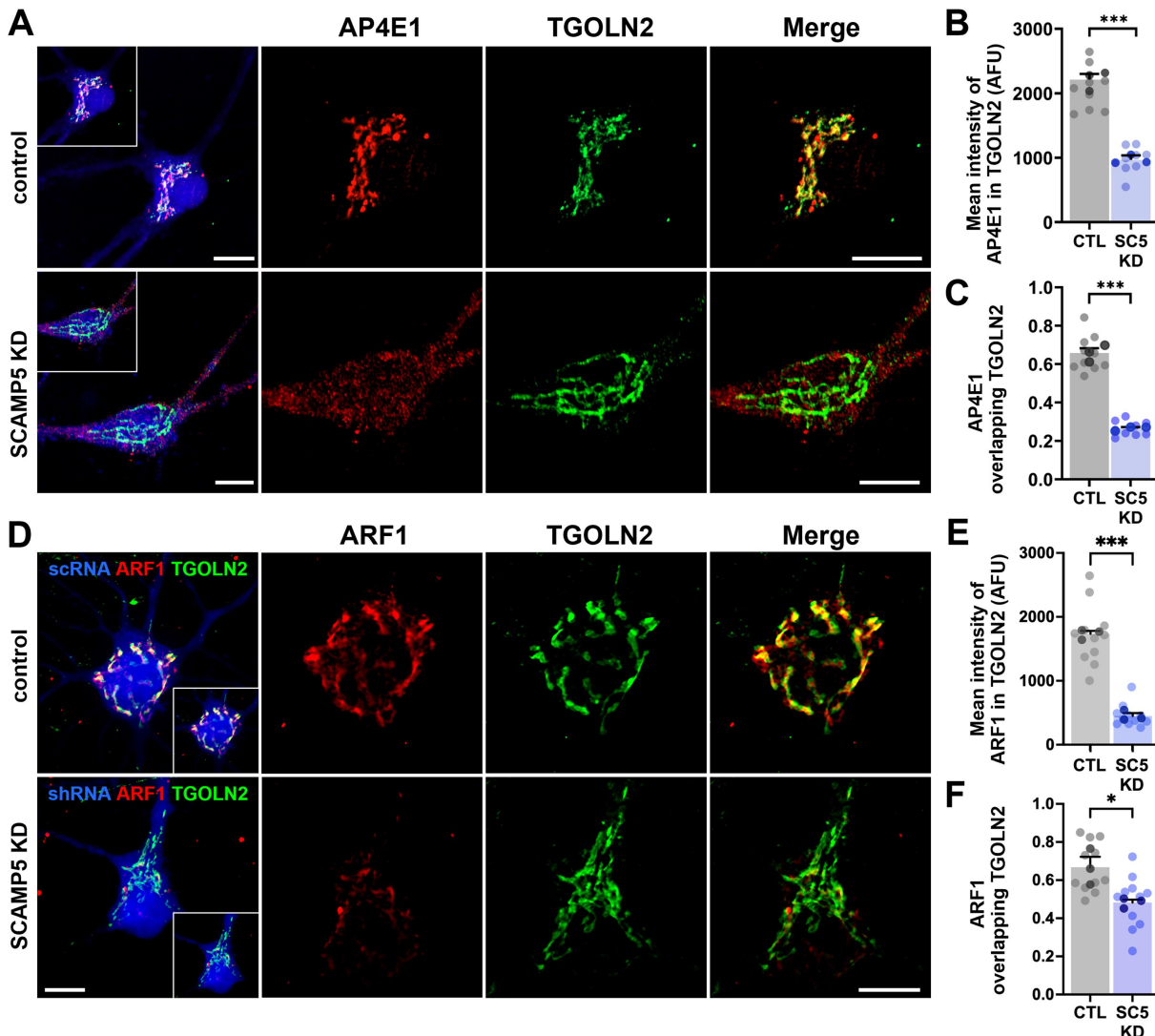


Figure 3. SCAMP5 knockdown causes defects in AP-4 and ARF1 recruitment to the TGN in neurons. (A) Representative Airyscan super-resolution images of cultured rat hippocampal neurons transfected with scRNA or shRNA of *Scamp5*, followed by immunostaining with anti-AP4E1 and anti-TGOLN2/TGN38 antibodies. Scale bar: 25 μ m; 5 μ m. (B) mean intensity of AP4E1 immunoreactivity in control and SCAMP5 KD (SC5 KD) neurons. CTL: 2210.84 \pm 88.431, n = 3 (10 neurons); SC5 KD: 996.02 \pm 40.124, n = 3 (9 neurons); p < 0.001, analyzed by Student's t-test. AFU, arbitrary fluorescence units. Values are indicated as mean \pm SEM. (C) Mander's colocalization coefficients show AP4E1 overlaps with TGOLN2. CTL: 0.66 \pm 0.025, n = 3 (10 neurons); SC5 KD: 0.27 \pm 0.012, n = 3 (9 neurons). p < 0.001, analyzed by Student's t-test. Values are indicated as mean \pm SEM. (D) Representative images of cultured rat hippocampal neurons transfected with scRNA or shRNA of SCAMP5, followed by immunostaining with anti-ARF1 and anti-TGOLN2/TGN38 antibodies. Scale bar: 25 μ m; 5 μ m. (E) mean intensity of ARF1 immunoreactivity in control and SCAMP5 KD neurons. CTL: 1734.01 \pm 46.845, n = 3 (11 neurons); SC5 KD: 450.17 \pm 46.055, n = 3 (11 neurons); p < 0.001, analyzed by Student's t-test. AFU, arbitrary fluorescence units. Values are indicated as mean \pm SEM. (F) Mander's colocalization coefficients showing ARF1 overlap with TGOLN2. CTL: 0.67 \pm 0.055, n = 3 (11 neurons); SC5 KD: 0.48 \pm 0.016, n = 3 (11 neurons); p = 0.031, analyzed by Student's t-test. Each shaded point represents data from a single neuron, and each filled point represents the mean of each independent experiment. Values are indicated as mean \pm SEM. * p < 0.05, *** p < 0.001.

both N- and C-termini (TM2–2/3-TM3) showed no binding affinity (Figure 4H). We also found that a mutant lacking the N-terminal region (Δ Nt) failed to bind to AP4M1 whereas a YXXΦ motif mutant (AXXAA) at the N-terminal region of SCAMP5 [50] binds to AP4M1 (Figure 4I). Collectively, these results suggest that the distinct motif formed by the N-terminal region with the first transmembrane domain is necessary for the interaction between SCAMP5 and AP4M1.

Although AP-4 interacts with SCAMP5, we found that shRNA-mediated knockdown of ARF1, validated in rat hippocampal neurons (Figures S7A-D), resulted in a significant reduction in colocalization between AP-4 and TGOLN2 (Figures S7E-G). Furthermore, we demonstrated that overexpression of dominant-negative ARF1 T-31N

mutants caused a significant reduction in AP-4 levels at the TGN (Figures S7H-J). These results indicate that without ARF1, AP-4 recruitment to the TGN is significantly impaired, demonstrating that SCAMP5-mediated AP-4 localization at the TGN requires ARF1.

SCAMP5 KD results in impaired localization of ATG9A at the presynaptic terminals and increased accumulation of ATG9A at the TGN

ATG9A is a specific AP-4 cargo, and AP-4 mediates the export of ATG9A from the TGN to promote autophagosome formation [16,50]. Recent studies also found that the impaired

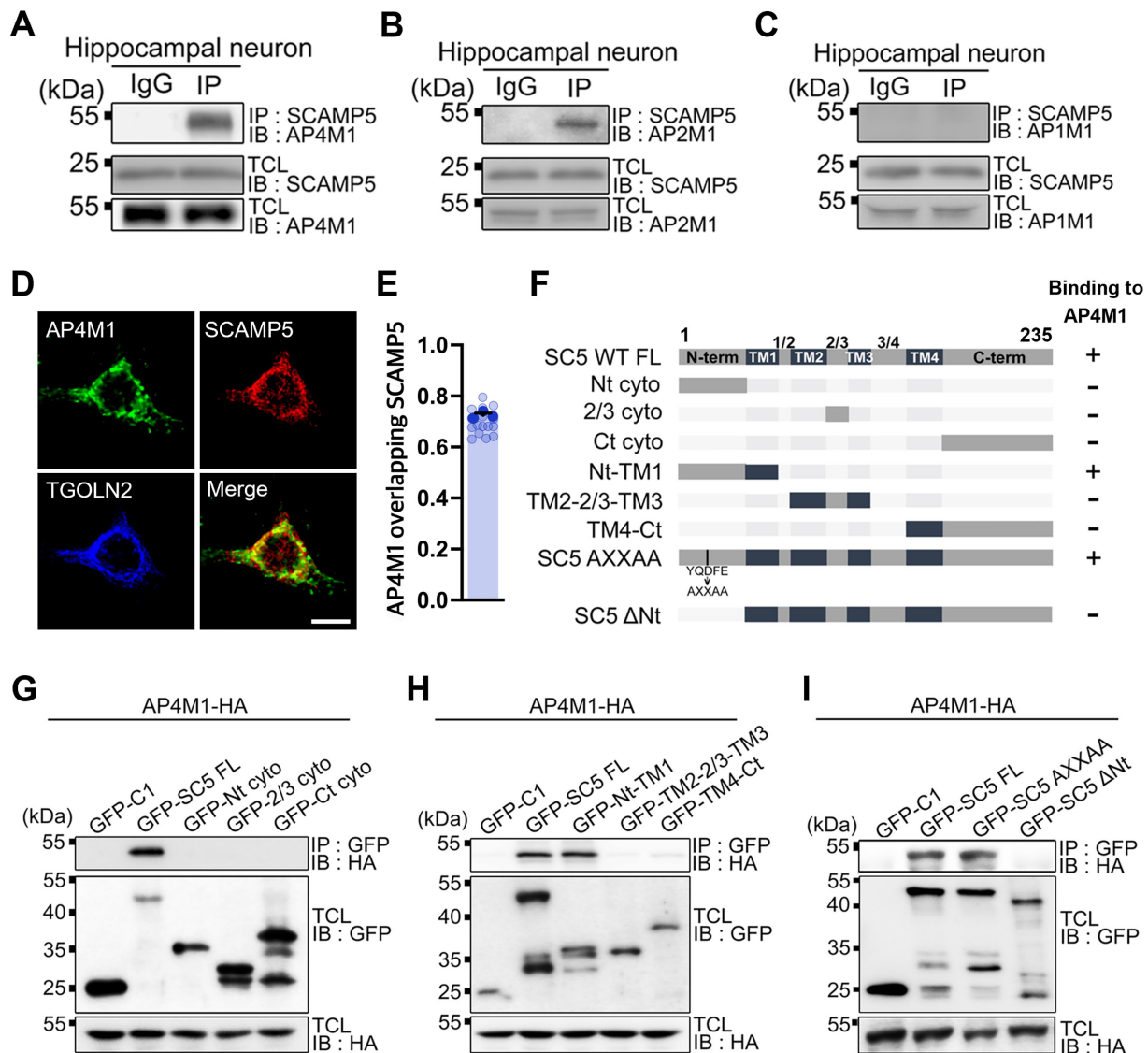


Figure 4. SCAMP5 interacts with AP4M1 in the hippocampal neurons. (A-C) neurons were lysed and immunoprecipitated using anti-immunoglobulin G (IgG, 1st lane) and anti-SCAMP5 (2nd lane) antibodies, followed by immunoblotting with anti-AP4M1 antibody (A), anti-AP2M1 antibody (B), or anti-AP1M1 antibody (C). (D) Representative images of neurons that were transfected with AP4M1-EGFP and immunostained with anti-SCAMP5 and anti-TGOLN2/TGN38 antibodies. Scale bar: 5 μ m. (E) Mander's colocalization coefficients revealed that AP4M1 overlaps with SCAMP5 in 0.73 ± 0.008 , $n = 3$ (16 neurons). Values are represented as mean \pm SEM. (F) schematic figures SCAMP5 mutant constructs used in the experiments. "+" or "-" marks indicate whether each construct binds to AP4M1. Nt: N-terminal region; TM: transmembrane domain; 2/3: 2/3 loop domain; Ct: C-terminal region; cyto: cytoplasmic domain. (G-I) HA-tagged AP4M1 and EGFP-tagged SCAMP5 mutant constructs were expressed in HEK-293T cells, followed by cell lysis and immunoprecipitation using an anti-GFP antibody, followed by immunoblotting with anti-HA antibody. Scamp5.

ATG9A localization at synapses is associated with defects in activity-induced presynaptic autophagy [16,39,40].

We found defects in autophagosome formation at presynaptic terminals in SCAMP5 KD neurons (Figure 1). Additionally, defects in the recruitment of PI4KB and PtdIns4P production impaired the recruitment of AP-4 at the TGN in SCAMP5 KD neurons (Figures 2 and 3). These results strongly imply that SCAMP5 KD disrupts AP-4-mediated ATG9A export at the TGN and impedes its trafficking along the axon to the presynaptic terminals. To investigate this possibility, we first conducted co-transfection of mRFP-ATG9A and EGFP-SYP with mTagBFP2-scrambled RNA or shRNA targeting *Scamp5* in rat hippocampal neurons (Figure 5A). We found a marked reduction in the number of ATG9A with SCAMP5 KD, while the levels of SYP remained

unaffected (Figure 5C,D). Additionally, the colocalization between SYP and ATG9A was significantly decreased, suggesting that SCAMP5 KD hampers the axonal trafficking and presynaptic localization of ATG9A (Figure 5A,E). Co-expressing a shRNA-resistant form of wild-type SCAMP5 (SC5 RES) fully rescued the observed impairments in ATG9A trafficking and localization to presynaptic boutons (Figure 5B-E).

We then conducted immunocytochemistry to investigate the endogenous localization of ATG9A in control and SCAMP5 KD, as well as *ap4m1* KO neurons that we established using the CRISPR-Cas9 system (Figures 6 and 7 and Figure S8-9). ATG9A displayed a distinct vesicular distribution pattern in control neurons, with a portion colocalizing with TGOLN2 (Figure 6A), consistent with a previous study [16]. In contrast, both SCAMP5 KD and *ap4m1* KO neurons

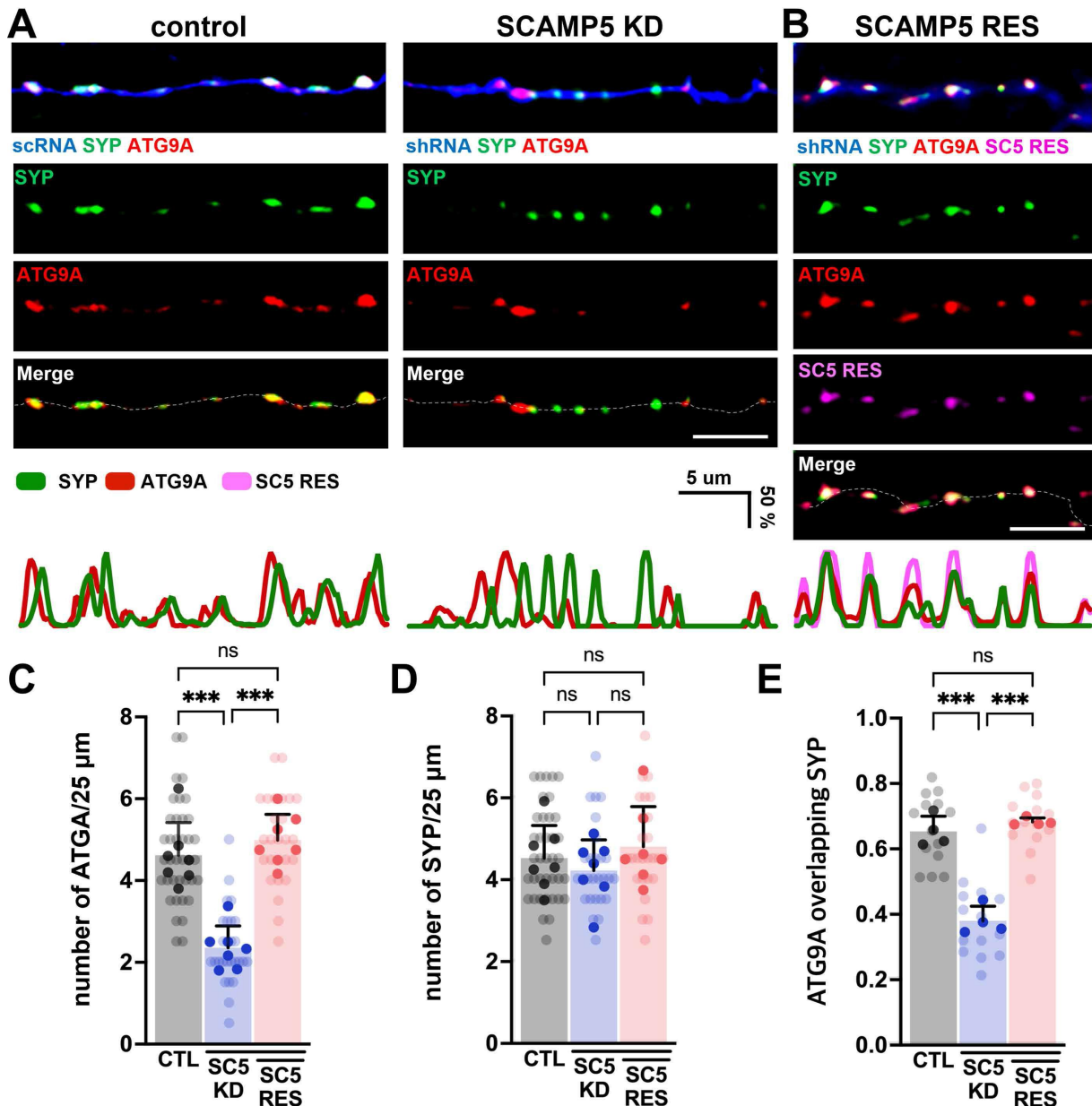


Figure 5. SCAMP5 depletion impairs the localization of ATG9A at presynaptic terminals. (A-B) Representative images of cultured rat hippocampal neurons co-transfected with mRFP-ATG9A, EGFP-SYP, and either mTagbfp2-scRNA (control), shRNA of *Scamp5* (SCAMP5 KD), or HA-shRNA-resistant form of SCAMP5 (SC5 RES). Scale bar: 5 μm. The bottom traces show line-scan profiles for each experimental condition (A-B) to quantify colocalization between ATG9A and SYP (red: ATG9A, green: SYP, magenta: SC5 RES). (C) The number of ATG9A puncta along a 25 μm segment of the axon. CTL: 4.62 ± 0.302, n = 7 (38 axons); SC5 KD: 2.36 ± 0.201, n = 7 (27 axons); SC5 RES: 4.99 ± 0.238, n = 7 (26 axons); p < 0.001. Values are indicated as mean ± SEM. (D) The number of SYP puncta along a 25 μm segment of the axon. CTL: 4.53 ± 0.302, n = 7 (38 axons); SC5 KD: 4.22 ± 0.285, n = 7 (27 axons); SC5 RES: 4.81 ± 0.370, n = 7 (26 axons); p = 0.7586. Values are indicated as mean ± SEM. (E) Mander's colocalization coefficients show ATG9A overlaps with SYP. CTL: 0.65 ± 0.023, n = 4 (14 axons); SC5 KD: 0.38 ± 0.220, n = 4 (14 axons); SC5 RES: 0.68 ± 0.006, n = 4 (14 axons); p < 0.001. Values are indicated as mean ± SEM. n represents the number of independent experiments with each experiment analyzing 3–5 neurons. Each shaded point represents data from a single neuron, and each filled point represents the mean of each independent experiment. Data were analyzed by one-way ANOVA followed by Tukey HSD post hoc test. ***p < 0.001, ns: not significant.

showed a notable increase in ATG9A accumulation along tubule-like structures at the TGN (Figure 6A–F). We observed that *ap4m1* KO neurons exhibited a higher accumulation of ATG9A compared to SCAMP5 KD neurons. This higher accumulation in *ap4m1* KO neurons could be attributed to the upregulation of ATG9A protein synthesis following *ap4* KO (~3-fold increase; Figures S8E and F). This is consistent with previous reports showing a 3 ~ 4-fold increase in ATG9A synthesis upon AP4 KO [37,39,61]. In contrast, SCAMP5 KD induces a moderate increase in ATG9A protein synthesis

(~1.4-fold increase; Figures S6A and B). The simultaneous knockdown/knockout of SCAMP5 and AP4M1 did not further exacerbate ATG9A accumulation beyond that observed with *ap4m1* KO alone (Figure 6D,F). These results suggest that although ATG9A expression increases in SCAMP5 KD and *ap4* KO neurons, the bulk of ATG9A remains confined to the TGN.

Accumulation of endogenous ATG9A at the TGN upon SCAMP5 KD and *ap4m1* KO suggests the defects in ATG9A export at the TGN and subsequent trafficking along the

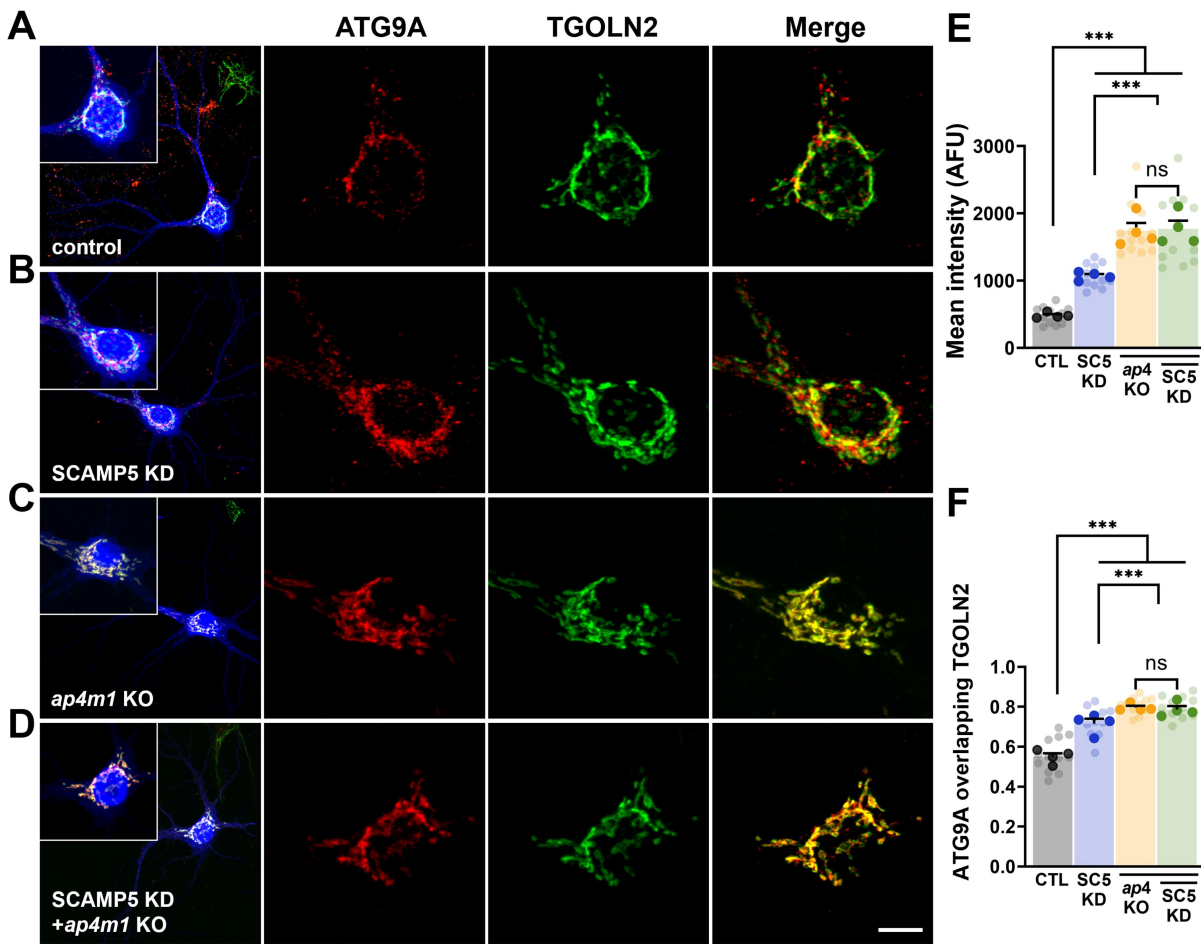


Figure 6. Endogenous ATG9A accumulates in the TGN of both SCAMP5 knockdown and *ap4m1* knockout neurons. (A-D) Representative images of cultured rat hippocampal neurons transfected with either mTagbfp2-tagged *Scamp5*-scRNA (control, A), *Scamp5*-shRNA (SCAMP5 KD, B), *ap4m1*-sgRNA for knockout (*ap4m1* KO, C) or *Scamp5*-shRNA with *ap4m1*-sgRNA (SCAMP5 KD+ *ap4m1* KO, D), followed by immunostaining with anti-ATG9A and anti-TGOLN2/TGN38 antibodies. Scale bar: 25 μ m; 5 μ m. (E) mean intensity of ATG9A in control, SCAMP5 KD, *ap4m1* KO, and SCAMP5 KD + *ap4m1* KO neurons. CTL: 482.00 ± 20.419, n = 4 (12 neurons); SC5 KD: 1067.64 ± 30.453, n = 4 (12 neurons); *ap4m1* KO: 1741.68 ± 116.837, n = 4 (12 neurons); SC5 KD + *ap4m1* KO: 1769.07 ± 121.917, n = 4 (12 neurons); p < 0.001. AFU, arbitrary fluorescence units. Values are indicated as mean ± SEM. (F) Mander's colocalization coefficients revealed that ATG9A overlaps with TGOLN2. CTL: 0.55 ± 0.017, n = 4 (12 neurons); SC5 KD: 0.72 ± 0.025, n = 4 (12 neurons); *ap4m1* KO: 0.80 ± 0.009, n = 4 (12 neurons); SC5 KD + *ap4m1* KO: 0.79 ± 0.017, n = 4 (12 neurons); p < 0.001; p = 0.025. Values are indicated as mean ± SEM. n represents the number of independent experiments with each experiment analyzing 3 neurons. Each shaded point represents data from a single neuron, and each filled point represents the mean of each independent experiment. Data were analyzed by one-way ANOVA followed by Tukey HSD post hoc test. ***p < 0.001, ns: not significant.

axon to the presynaptic terminals (Figures 6 and 7). The simultaneous knockdown/knockout of SCAMP5 and AP4M1 did not exacerbate ATG9A trafficking defects compared to the individual manipulations (see Figure 6D,F). We also noticed that, unlike transiently expressed mRFP-ATG9A, which led to decreased axonal ATG9A spots with SCAMP5 KD (Figure 7B), we observed ectopic ATG9A spots along the axons in *ap4m1* KO neurons (Figure 7C). However, most of these spots did not colocalize with SYP, except in control neurons (Figure 7A-F). These effects could again be attributed to the upregulation of ATG9A protein synthesis following *ap4* KO. Consistent with this interpretation, a previous study showed that *ap4* KO leads to increased ATG9A expression, causing a leakage of ATG9A

from the TGN to the axons via AP-4-independent mechanisms [16]. Collectively, our results from transient expression and endogenous staining of ATG9A indicate that, upon SCAMP5 KD, ATG9A accumulates at the TGN, resulting in defects in its axonal trafficking and presynaptic localization.

The turnover of presynaptic proteins is impaired with SCAMP5 KD

Presynaptic autophagy serves to eliminate dysfunctional and aged proteins from distal presynaptic terminals, and when impaired, it can have significant repercussions on synaptic function and ultimately neuronal survival [61,66]. Our results

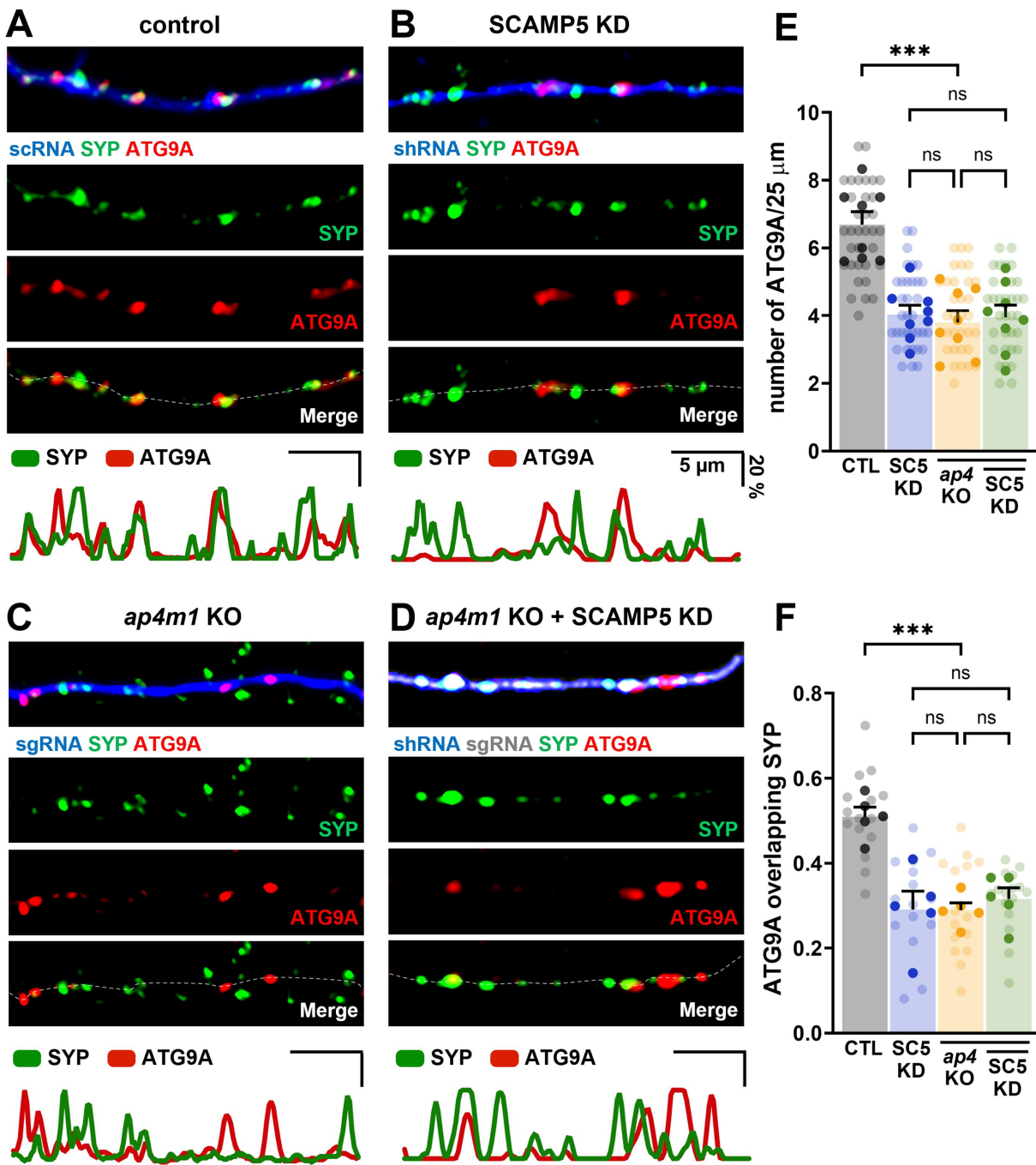


Figure 7. Defects in ATG9A trafficking along the axon to the presynaptic terminals are observed in both SCAMP5 knockdown and *ap4m1* knockout neurons. (A-D) Representative images of cultured rat hippocampal neurons co-transfected with mCherry-SYP, either mTagbfp2-*Scamp5* scRNA (control, A), mTagbfp2-*Scamp5*-shRNA (SCAMP5 KD, B), EGFP-*ap4m1*-sgRNA (*ap4m1* KO, C), or mTagbfp2-*Scamp5*-shRNA with EGFP-*ap4m1*-sgRNA (SCAMP5 KD + *ap4m1* KO, D), followed by immunostaining with anti-ATG9A antibody to detect endogenous localization of ATG9A. Scale bar: 5 μm. The bottom traces show line-scan profiles for each experimental condition (A-D) to quantify colocalization between endogenous ATG9A and mCherry-SYP (red: ATG9A, green: SYP). (E) the number of endogenous ATG9A puncta along a 25 μm segment of the axon. CTL: 6.69 ± 0.380 , n = 8 (34 axons); SC5 KD: 4.03 ± 0.275 , n = 8 (34 axons); *ap4m1* KO: 3.80 ± 0.348 , n = 8 (34 axons); SC5 KD + *ap4m1* KO: 3.95 ± 0.360 , n = 8 (34 axons); p < 0.001. Values are indicated as mean ± SEM. (F) Mander's colocalization coefficients show endogenous ATG9A overlap with mCherry-SYP. CTL: 0.51 ± 0.023 , n = 5 (16 axons); SC5 KD: 0.29 ± 0.043 , n = 5 (16 axons); *ap4m1* KO: 0.29 ± 0.017 , n = 5 (16 axons); SC5 KD + *ap4m1* KO: 0.32 ± 0.026 , n = 5 (16 axons); p < 0.001. Values are indicated as mean ± SEM. n represents the number of independent experiments with each experiment analyzing 3–5 neurons. Each shaded point represents data from a single neuron, and each filled point represents the mean of each independent experiment. Data were analyzed by one-way ANOVA followed by Tukey HSD post hoc test. ***p < 0.001, ns: not significant.

so far imply that SCAMP5 KD potentially hampers the autophagy-mediated turnover of presynaptic proteins at the presynaptic terminals.

To test this hypothesis, we deployed a medium fluorescent timer (mFT) fused to the synaptic vesicle protein SV2A/SV2

(mFT-SV2) [67] (Figure 8A–D). The mFT-SV2 construct allowed us to monitor the age of SV proteins at individual synapses by measuring the red:blue fluorescent intensity ratio, which transitions from blue to red over time [68]. In SCAMP5 KD neurons, while we observed comparable blue signals,

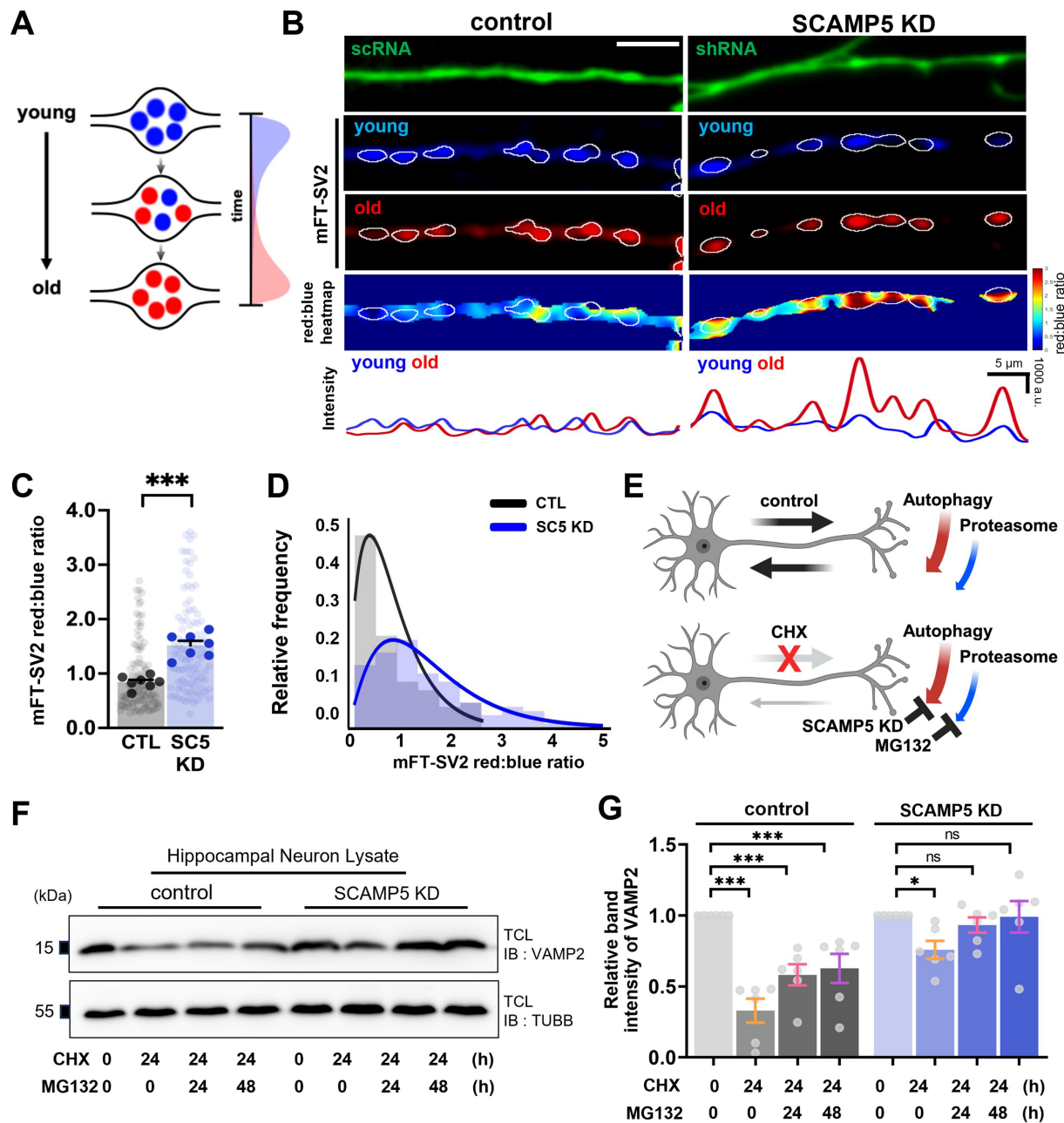


Figure 8. The turnover of presynaptic proteins is impaired with SCAMP5 KD. (A) Schematic figure of mFT-tagged synaptic vesicle protein SV2/SV2A, where mFT undergoes a time-dependent change in its fluorescence from blue to red. (B) Representative images of cultured rat hippocampal neurons co-transfected with mFT-SV2 and either EGFP-*Scamp5*-scRNA (control) or *Scamp5*-shRNA (SCAMP5 KD). The bottom panels display heatmaps of red:blue fluorescence intensity ratios and corresponding line-scan profiles for control and SCAMP5 KD neurons, enabling precise quantification and spatial mapping of signal distribution differences between the red and blue channels. Scale bar: 5 μm. (C) The ratio (fluorescence intensities) between old (red) and young (blue) mFT-SV2 in control and SCAMP5 KD. CTL: 0.84 ± 0.043 , $n = 7$ (100 boutons); SCAMP5 KD: 1.52 ± 0.083 , $n = 7$ (100 boutons); $p < 0.001$, analyzed by Student's *t*-test. Values are indicated as mean \pm SEM. (D) The frequency histogram of the normalized red:blue ratio in control and SCAMP5 KD. n represents the number of independent experiments, with each experiment analyzing 3 neurons. (E) An experimental scheme of cycloheximide (CHX) chase assay. (F) Control or SCAMP5 KD neurons were treated with DMSO, CHX alone for 24 h, or with CHX in combination with MG132 for 24 or 48 h (CHX+MG132), then lysed, and immunoblotted with anti-VAMP2 antibody. (G) Quantification of VAMP2 band intensity following CHX or CHX+MG132 treatment, normalized to DMSO-treated samples within each control and SCAMP5 KD neurons ($n = 5$ independent experiments). CTL: CHX: 0.33 ± 0.084 ($p < 0.001$); CHX +24 h MG132: 0.58 ± 0.074 ($p < 0.001$); CHX +48 h MG132: 0.63 ± 0.102 ($p < 0.001$); SC5 KD: CHX: 0.75 ± 0.063 ($p = 0.038$); CHX +24 h MG132: 0.93 ± 0.053 ($p = 0.981$); CHX +48 h MG132: 0.99 ± 0.111 ($p > 0.999$). Each shaded point represents data from a single neuron, and each filled point represents the mean of each independent experiment. Values are indicated as mean \pm SEM. Data were analyzed by one-way ANOVA followed by Tukey HSD post hoc test. ** $p < 0.01$, *** $p < 0.001$, ns: not significant.

there was a significant increase in the red signal relative to the blue signal (older protein over newer protein) at the majority of synapses compared to control neurons, which resulted in a significantly higher mFT-SV2 red:blue ratio. These results

indicate impaired SV2 protein degradation and turnover in SCAMP5 KD neurons relative to controls (Figure 8A–D).

Furthermore, we substantiated the impaired protein turnover using a cycloheximide (CHX) chase assay (Figure 8E–G).

Upon inhibition of protein synthesis by CHX, intracellular protein levels decrease through degradation via the proteasomal and lysosomal pathways, including autophagy. We found that in control neurons, the SV protein VAMP2 degraded to approximately 70% of its initial levels within 24 h after CHX treatment. In contrast, VAMP2 levels in SCAMP5 KD neurons were largely maintained, showing only a slight decrease (~25%), indicating impaired degradation of VAMP2. The slight but statistically significant decrease in VAMP2 levels observed in SCAMP5 KD neurons implies the involvement of an alternative proteasomal degradation pathway. To test this hypothesis, we repeated the CHX chase assay in the presence

of the proteasome inhibitor MG132. When neurons were co-treated with MG132 and CHX for 24 h, VAMP2 levels decreased to ~45% of their initial levels, compared to the ~70% reduction observed with CHX alone; prolonged incubation with MG132 for 48 h did not induce further reduction. In SCAMP5 KD neurons, the slight decrease in VAMP2 levels with CHX alone was restored to control levels upon co-administration of MG132 and CHX. These findings suggest that the majority of VAMP2 degradation is mediated by autophagy, while a minor portion is mediated by the proteasomal pathway.

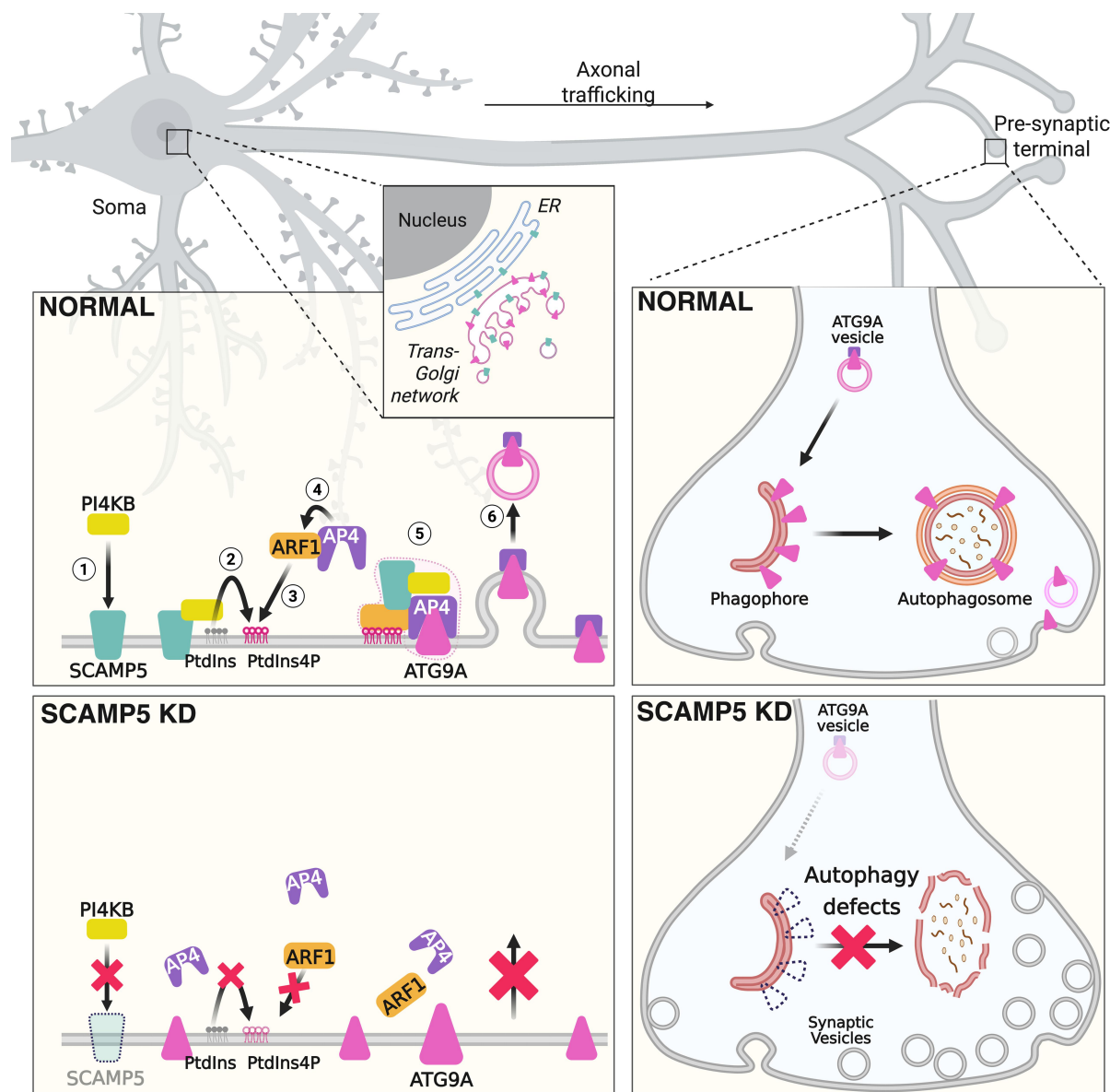


Figure 9. Proposed working model of SCAMP5 in regulating presynaptic autophagy. Based on our results, we propose the following model for SCAMP5's role in presynaptic autophagy. SCAMP5 interacts with and recruits PI4KB to the TGN, where PI4KB produces PtdIns4P. This localized PtdIns4P production is essential for recruiting ARF1 to the TGN, which in turn facilitates AP-4 localization. Although SCAMP5 directly interacts with AP-4, we hypothesize that this interaction serves to stabilize AP-4 at the TGN after ARF1-mediated recruitment, rather than directly recruiting AP-4. When SCAMP5 is knocked down, PI4KB recruitment to the TGN is disrupted, leading to impaired localized PtdIns4P production and significantly decreased PtdIns4P levels. Consequently, both ARF1 and AP-4 recruitment to the TGN are impaired, which hinders ATG9A export from the TGN and causes its accumulation. This disruption in ATG9A trafficking from the TGN to axons ultimately impairs presynaptic autophagosome formation, leading to defective presynaptic autophagy and the accumulation of aged synaptic vesicle proteins.

Taken together, these findings collectively underscore the crucial role of SCAMP5 in AP-4-mediated ATG9A export and trafficking to the presynaptic terminals, and when impaired, these processes lead to defects in autophagosome formation and subsequent impaired protein homeostasis at the presynaptic terminals.

Discussion

Our investigation elucidates the functional significance of SCAMP5 enrichment at the TGN. We demonstrate that SCAMP5 interacts with PI4KB, thereby modulating PI4KB recruitment and subsequent PtdIns4P production at the TGN. This process is critical for the recruitment of AP-4 and ARF1 to the TGN. Given that AP-4 facilitates the presynaptic export of ATG9A from the TGN, we observed that SCAMP5 knockdown or disruption of the SCAMP5-AP4M1 interaction significantly impedes the axonal trafficking of ATG9A-containing vesicles. Consequently, this impairment leads to compromised presynaptic autophagy and altered turnover of synaptic vesicle proteins (Figure 9). These findings collectively underscore the pivotal role of SCAMP5 in orchestrating presynaptic autophagy through its regulatory effects on PtdIns4P production and ATG9A trafficking.

Presynaptic terminals, being highly dynamic compartments, rely on presynaptic autophagy to selectively remove damaged organelles and toxic proteins, preventing their accumulation during synaptic activity [40,41,69]. This process regulates synaptic strength by modulating the number and efficacy of synaptic connections and is itself triggered by synaptic activity [70]. Our data demonstrate the functional importance of SCAMP5 in maintaining proper presynaptic autophagy. Combined with our previous findings on SCAMP5's role in facilitating endocytosis and promoting efficient synaptic vesicle clearance during high neuronal activity, these results suggest that SCAMP5 may serve as a critical safeguard, enabling neurons to withstand periods of intense synaptic activity.

Recent studies indicate interconnections between the synaptic vesicle cycle and autophagy at presynaptic terminals. Key endocytic proteins, including SYNJ1 [34], SH3GL family [32], and components of clathrin-mediated endocytosis – such as clathrin, DNM (dynamin), and RAB5A/RAB5 [66] – have been implicated in regulating synaptic autophagy and autophagosome formation. Furthermore, ESCRT proteins interact with autophagy receptors SQSTM1/p62 to facilitate selective degradation of ubiquitinated proteins [71]. Our findings suggest that SCAMP5, while primarily involved in exo-endocytosis at presynaptic terminals, also functions at the TGN, potentially modulating presynaptic autophagy. SCAMP5 plays a crucial role in synaptic vesicle endocytosis during high neuronal activity and participates in the exocytic pathway in the striatum [49,57]. SCAMP5 regulates release site clearance through interaction with the AP-2 complex [50] and modulates quantal size in glutamatergic neurons by mediating SLC9A6 axonal trafficking and presynaptic localization [51,56]. Our current study reveals that SCAMP5 also regulates presynaptic autophagy by influencing PtdIns4P production

and subsequent AP-4-dependent export and axonal trafficking of ATG9A. SCAMP5 is highly enriched at the TGN and presynaptic terminals but is scarcely found in dendritic compartments. Our observations elucidate the multifaceted role of SCAMP5 in the regulation of presynaptic functions and the maintenance of synaptic protein homeostasis. Our findings suggest that SCAMP5 serves as a key molecular nexus, integrating vesicle trafficking dynamics with protein turnover mechanisms, thereby ensuring optimal presynaptic performance. This intricate balance is essential for sustaining synaptic efficacy and plasticity.

Our findings contrast with a previous study demonstrating that SCAMP5 overexpression increased LC3-II accumulation in HEK-293T and SH-SY5Y cells, leading to the interpretation that SCAMP5 inhibits autophagosome-lysosome fusion [58]. While we observed reduced autophagosome formation at presynaptic boutons following SCAMP5 knockdown, the previous study showed decreased LC3-II levels upon SCAMP5 depletion in cell lines. Several key differences may account for this discrepancy. First, their experiments employed non-neuronal HEK-293T cells and neuroblastoma SH-SY5Y cells, which lack functional presynaptic terminals and the specialized synaptic vesicle trafficking machinery and exo-endocytic mechanisms essential for neurotransmission. Second, presynaptic autophagy represents a spatially restricted, activity-dependent process distinct from general cellular autophagy. Third, our cycloheximide chase experiments demonstrate that autophagy-dependent degradation is the major pathway for synaptic vesicle protein turnover, while proteasomal degradation plays a minor role. This contrasts sharply with most non-neuronal cell types, where the ubiquitin – proteasome system typically dominates protein degradation, particularly for short-lived, misfolded, or regulatory proteins, while autophagy primarily handles long-lived proteins, protein aggregates, and organelles. These differences suggest that SCAMP5's role in autophagy is highly compartment specific. While it may regulate general membrane trafficking in non-neuronal cells, SCAMP5 appears essential for autophagosome formation specifically at presynaptic terminals, and its function cannot be extrapolated across distinct cellular environments.

SCAMP isoforms are suggested to have distinct trafficking pathways mediated by selective interactions with adaptor proteins [72]. One study revealed significant colocalization of SCAMP2 with the AP-1 adaptor complex, particularly at perinuclear Golgi compartments, suggesting its potential role in AP-1-mediated vesicle formation in these regions. Similarly, SCAMP3 displayed strong colocalization with the AP-3 adaptor complex, especially at perinuclear sites [45]. Our previous work showed that SCAMP5 interacts with AP-2 at the presynaptic membrane, critical for its role in clearing release sites [50]. Here, we further demonstrate that SCAMP5 binds to AP-4 but not AP-1 at the TGN, highlighting how different SCAMP isoforms mediate distinct trafficking pathways depending on their localization within the cytoplasm. Deficiency in AP-4 leads to a depletion of axonal ATG9A, highlighting its dependence on AP-4 for proper delivery to presynaptic terminals [39,61,73]. Additionally, AP-4 vesicles deliver ATG9A to the cell periphery, necessary for autophagosome formation. Notably, RUSC1 and RUSC2 proteins are required for recruiting AP-4 vesicles to

ATG9A-positive membranes [17]. Of note, despite a direct interaction between SCAMP5 and AP-4, we found that without ARF1, AP-4 recruitment to the TGN is severely impaired (Figure S7). We hypothesized that SCAMP5 interaction with AP-4 acts as a means of stabilizing AP-4 at the TGN once it has been recruited via ARF1, rather than directly recruiting AP-4 to the TGN. Impaired autophagosome formation within axons due to AP-4 deficiency disrupts proper axonal extension and leads to the development of distal axonal swellings. These swellings accumulate endoplasmic reticulum, ultimately compromising axonal integrity in AP-4 deficiency syndrome [39]. Our findings suggest that SCAMP5 deficiency or dysfunction at the TGN may result in a phenotype that mimics the symptoms associated with AP-4 deficiency, suggesting a common underlying pathophysiology, potentially involving disrupted protein trafficking and autophagy regulation at presynaptic terminals. Given that de novo mutations and copy number variations in the SCAMP5 gene have been implicated in neurodevelopmental disorders, including autism spectrum disorder (ASD) and intellectual disability [46,74], our results highlight the need for further investigation into the potential mechanistic links between these disorders and impairments in presynaptic autophagy and AP-4-dependent cellular processes.

Recent studies reveal that ATG9A localizes to a distinct population of vesicles with a slightly larger diameter than those positive for SYP, a marker for synaptic vesicles [40,73]. Proteome analysis using label-free quantification mass spectrometry combined with super-resolution microscopy revealed ATG9A as a largely distinct vesicle pool at the presynapse that exhibits only limited overlap with the SVs containing SYP [73]. This strongly suggests the existence of separate vesicular sorting and trafficking pathways for these two proteins. Although proteome analysis revealed the high enrichment of several proteins including SCAMP5 in ATG9A-containing vesicles [73], and our results showed impaired ATG9A trafficking – but not SYP levels – following SCAMP5 knockdown (Figure 5), it remains unclear whether SCAMP5 is co-transported with ATG9A in ATG9A-containing vesicles or, as a bona fide SV protein, follows the conventional SV protein trafficking pathway. This question requires further investigation. Another important point is that ATG9A-containing vesicles exhibit significant heterogeneity in their membrane composition [75]. This heterogeneity may originate from the diverse sites of vesicle formation, such as the TGN, where the incorporation of different proteins during vesicle budding could contribute to variability. Alternatively, it may result from imprecise sorting mechanisms during vesicle biogenesis or the random engagement of different adaptor proteins, such as AP-2 and AP-4, at the TGN. Future research is needed to determine whether this heterogeneity has functional implications in autophagy and to explore potential differences in the trafficking routes of these subpopulations.

The observed association of impaired autophagy with synaptic dysfunction in neurological disorders like Parkinson disease, Alzheimer disease, autism spectrum disorders, and epilepsy highlights the critical link between autophagy and synaptic health [76–80]. Interestingly, two specific missense mutations (R91W and G180W) in SCAMP5 have been identified in individuals with

neurodevelopmental disorders characterized by autistic features and seizures [48]. Additionally, SCAMP5 deficiency has been linked to pediatric epilepsy and juvenile Parkinson disease [46–48]. While the exact mechanisms by which these mutations trigger disease development remain unclear, a common thread linking these pathologies is a deficiency in autophagy [57,60,61]. Given SCAMP5's critical role in regulating presynaptic autophagy, these mutations may indirectly disrupt autophagic flux within synapses, which could be a contributing factor in the pathological mechanisms of these diseases. Further investigation using SCAMP5 mutation models holds promise for developing therapeutic interventions targeting neurodevelopmental disorders associated with these mutations and concomitant autophagy dysfunction.

Materials and methods

Plasmid DNA construction

Full-length or domain fragments of EGFP-tagged or GST-tagged rat *Scamp5* cDNA (NM-031726) constructs and small hairpin RNA (shRNA) for *Scamp5* were made as previously reported [51]. AP4M1-HA and ARF1-HA constructs were generated by insertion of the HA epitope at the C-terminal region of the human *AP4M1* and *ARF1* cDNA (purchased from Korea Human Gene Bank, Medical Genomics Research Center, KRIBB, BKU001904 [*AP4M1*]; BKU008414 [*ARF1*]). All of the missense or nonsense mutation constructs of SCAMP5 and ARF1 were made by site-directed mutagenesis. The target sequence for *ap4m1* knockout (KO) based on the CRISPR-Cas9 system was predicted by CCTOP [81,82]. sgRNA-targeting *ap4m1* exon 1: 5'-CCTTCTTGCTTACTTCTTGA-3' was cloned into pSpCas9(BB)-2A-GFP (PX458-GFP; Addgene 48,138; deposited by Feng Zhang) or 1179_pAAV-U6-BbsI-gRNA-CB-EmGFP (Addgene 89,060; deposited by William Lagor) as described in the Zhang Lab General Cloning Protocol [83–86]. spCas9 was subcloned into the pAAV.hSyn-empty vector (gifted from Dr. Won-Kyung Ho, Seoul National University College of Medicine). The *Arf1*-targeting shRNA: 5'-GGGAAGACAACAATTCTAT-3' was designed with Biosettia's shRNA designer (<https://biosettia.com/support/shrna-designer/>) and was cloned into the pAAV-U6 shRNA vector (Cell Biolabs, VPK-413-DJ). The following plasmids were generously provided: FLAG-PI4KB (from Dr. Angelika Hausser, University of Stuttgart), pRSFD-His6-GB1-TEV site-PI4KB (residues 1–423 & 522–816) (from Dr. Dvzen Boura, IOCB Prague), EGFP-SYP (from Dr. Jane Sullivan, University of Washington), mNeonGreen-GOLGB1 (Addgene 98,880; deposited by Dr. Dorus Gadella), pMXs-puro-RFP-ATG9A (Addgene 60,609; deposited by Dr. Noboru Mizushima), and FU-mFT-SV2 (from Dr. Craig Garner, German Center for Neurodegenerative Diseases [DZNE]).

Antibodies

Anti-rabbit SCAMP5 (Abcam, ab3432), anti-mouse SYP/synaptophysin 1 (Synaptic Systems, 101 011), anti-mouse EEA1 (BD Biosciences 610,456), anti-mouse LAMP1

(Invitrogen, MA1-164), anti-mouse TGOLN2/TGN38 (BD Biosciences 610,898), anti-mouse TGOLN2/TGN46 (Invitrogen, MA3-063), anti-mouse PI4KB/PI4KIII β (BD Biosciences 611,816), anti-rabbit MAP1LC3B/LC3B (Sigma-Aldrich, L7543), anti-rabbit AP1M1 (Acris Antibodies, AP50198PU-N), anti-mouse AP2M1 (BD Biosciences 611,350), anti-rabbit AP4M1 (Invitrogen, PA5-22380), anti-rabbit TUBB/ β -tubulin (Abcam, ab6046), anti-mouse HA (BioLegend 901,514), anti-rat HA (Roche 11,867,431,001), anti-rabbit AP4E1 (Invitrogen, PA5-59775), anti-rabbit ATG9A (Abcam, ab108338), anti-rabbit ARF1 (Invitrogen, PA1-127), and anti-rabbit VAMP2 (Cell Signaling Technology 13,508) were used in the experiments. Anti-rabbit GFP antibody was custom-made by affinity purification by our laboratory. All horseradish peroxidase-conjugated secondary IgG antibodies (Jackson ImmunoResearch, 111-035-003 [anti-rabbit IgG]; 115-035-003 [anti-mouse IgG]) and Alexa Fluor secondary antibodies (Thermo Fisher Scientific, A21206 [anti-rabbit 488]; A10042 [anti-rabbit 568]; A32733 [anti-rabbit 647+]; A48265 [anti-rat 647+]; A48255 [anti-mouse 405+]; A32723 [anti-mouse 488+]; A11004 [anti-mouse 568]; A21237 [anti-mouse 647]) were used respectively in each experiment.

Cell lines culture and transfection

HEK-293T (ATCC, CRL-3216), HT-22 (provided by Dr. Won-Kyung Ho, Seoul National University College of Medicine), and HeLa (Korean Cell Line Bank 10,002) cell lines were maintained in Dulbecco's Modified Eagle's Medium (DMEM; WELGENE, LM 001-05) containing 10% fetal bovine serum (FBS; Gibco 12,483-020), 100 U/ml penicillin, and 100 μ g/ml streptomycin (WELGENE, LS202-02) at 37°C in 5% CO₂ humidified incubator. Cells were transfected with PEI-MAX (MW 40,000; Polysciences 24,765). For 90 mm culture dishes, 10 μ g of plasmid DNA was mixed with Opti-MEM (Gibco 31,985,070), combined mixture with 30 μ g PEI-MAX (1:3 ratio), and incubated for 20 min. For PI4KB gene knockdown, cells were transfected with ON-TARGETplus Human PI4KB siRNA (Horizon Discovery, L-006777-00) at a final concentration of 20 nM using Lipofectamine RNAiMAX (Invitrogen 13,778-075), according to the manufacturer's instructions. All of transfection mixtures were incubated with cells overnight, after which the medium was replaced with a fresh complete medium.

Rat primary hippocampal neuron culture and transfection

Animal experiments were approved by the Institute of Animal Care and Use Committee (IACUC; Approval ID number: SNU-220525-4) of Seoul National University, Korea. All experiments were carried out under approved guidelines and regulations. Primary rat hippocampal neurons derived from embryonic day 18 Sprague Dawley fetal rats of either sex was prepared as described previously [87]. Briefly, hippocampi were dissected, dissociated with papain (Worthington Biochemical Corporation, LS003119), and resuspended in minimal Eagle's medium (MEM; Hyclone,

SH30024.01) supplemented with 0.6% glucose, 1 mM pyruvate, 2 mM L-glutamine, and 10% fetal bovine serum (Gibco 12,483-020), and plated on Poly-D-lysine-coated glass coverslips in 60 mm Petri dishes. At 4 h after plating, the medium was replaced with a neurobasal medium (Gibco 12,348-017) supplemented with 2% B-27 (Gibco 12,587,010), 0.5 mM L-glutamine. Neurons were transfected by a modified calcium-phosphate method as previously described [87]. Briefly, 9 μ g of DNA and 10 μ L of 2.5 M CaCl₂ were mixed in distilled water to a total volume of 75 μ L and the same volume of 2x BBS (50 mM BES, 280 mM NaCl, and 1.5 mM Na₂HPO₄, pH 7.1) was added. The cell culture medium was completely replaced by transfection medium (MEM; 1 mM sodium pyruvate, 0.6% glucose, 10 mM HEPES, 1 mM Kynurenic acid, and 10 mM MgCl₂, pH 7.65), and the DNA mixture was added to the cells and incubated in a 5% CO₂ incubator for 60 min. Cells were washed with a washing medium (pH 7.30) and then returned to the original culture medium. Neurons were transfected at DIV 8–9 and analyzed at DIV 19–21.

Immunocytochemistry

Cultured rat hippocampal neurons were fixed in 4% paraformaldehyde with 4% sucrose in PBS (0.9% NaCl, 5.6 mM Na₂HPO₄, 1.06 mM KH₂PO₄, pH 7.3) for 15 min at room temperature (RT). Neurons were washed three times with PBS-G (50 mM glycine in PBS) and blocked with 10% bovine serum albumin (BSA; Bovogen, BSAS 0.1) or normal goat serum (NGS; Invitrogen, 01-6201) and 0.1% Triton X-100 (Sigma-Aldrich, T8787) in PBS for 1.5 h at RT. For AP4E1 and TGOLN2 co-staining (Figure 3A), neurons were fixed as above and subsequently permeabilized with pre-chilled methanol at -20°C for 5 min. After permeabilization, neurons were washed three times with PBS-G and blocked with 5% BSA in PBS containing 0.01% saponin for 30 min at RT. Primary antibodies diluted in the appropriate blocking solution (3% BSA or 5% NGS + 0.1% Tx-100/PBS or 5% BSA/PBS) were applied overnight at 4°C, followed by secondary antibodies in blocking solution for 45 min at 37°C. Coverslips were washed and mounted on slide glasses with an aqueous mounting medium (Dako, S3025).

Autophagy induction

Cultured rat hippocampal neurons were co-transfected with mTagBFP2-scRNA (sequence-scrambled shRNA) or shRNA of *Scamp5*, mCherry-SYP, and EGFP-LC3 at DIV 7 and treated with either 2 μ M Rapamycin (MedChemExpress, HY-10219) or 90 mM KCl (Sigma-Aldrich 60,128) for 10 min before imaging. Both Rapamycin and KCl were diluted in Tyrode's solution (136 mM NaCl, 2.5 mM KCl, 2 mM CaCl₂, 1.3 mM MgCl₂, 10 mM glucose, and 10 mM HEPES, pH 7.4, 285–290 mOsm).

Structure prediction

The three-dimensional protein structures of the SCAMP5 C-terminal region (PDB: Q8TAC9, residues 194–235) and

PI4KB N-terminal region (PDB: Q9UBF8, residues 1–67) shown in Figure 2 were predicted using AlphaFold3 in UCSF ChimeraX [88–90]. Since this PI4KB N-terminal region is known to bind the Q-rich domain of ACDB3 previously [64], we predicted putative contact sites (residues with atomic distance ≤ 4 Å) between the C-terminal Q-rich region of SCAMP5 and PI4KB N-terminal region. Molecular graphics and analyses were performed with UCSF ChimeraX [91,92].

Protein expression and purification

GST or 6xHis-MBP fusion proteins expressed in BL21 E. coli cells were induced with 0.5 mM isopropyl-1-thio-β-D-galactopyranoside (IPTG; Duchefa Biochemie, I1401) overnight at 30°C. Cells were lysed with Ni-NTA lysis buffer (50 mM NaH₂PO₄, pH 8.0, 300 mM NaCl, 10 mM imidazole [USB corporation 17,525]) for 6xHis proteins or hypotonic buffer (20 mM Tris-HCl, pH 7.4, 150 mM NaCl, 1 mM EGTA, 1 mM MgCl₂, and 0.25% Triton X-100) for GST proteins. After centrifugation at 14,000 ×g at 4°C for 20 min, supernatants were incubated with Ni-NTA Resin (Thermo Scientific 88,221) or Glutathione Agarose (Thermo Scientific 16,100) for 2 h. Proteins were eluted with Ni-NTA elution buffer (300 mM imidazole with Ni-NTA lysis buffer) or GST elution buffer (50 mM Tris-HCl, pH 7.4, 50 mM GSH [Sigma-Aldrich, G4251]) and stored at –80°C until use.

In vitro binding assay

6xHis-PI4KB and GST-SCAMP5-Ct were mixed with 200 μL of binding buffer (20 mM Tris-HCl, pH 8.0, 150 mM NaCl, 1 mM DTT) and incubated at 4°C on a rotator for 12 h. After adding Glutathione Agarose resin and incubating for 2 h, the resin was washed three times with 200 μL of binding buffer. Finally, the resin was boiled in sample buffer at 100°C for 5 min and analyzed by SDS-PAGE using 8–15% gradient gel, followed by Coomassie Brilliant Blue staining (0.025% Coomassie Brilliant Blue, 40% methanol, and 10% acetic acid).

Western blot and immunoprecipitation

Cells were lysed using 1% Triton X-100 lysis buffer (20 mM Tris-HCl, pH 8.0, 1% Triton X-100, 10% glycerol, 137 mM NaCl, 2 mM EDTA, 1 mM PMSF [Thermo Scientific 36,978], and 1x protease inhibitor cocktail [Sigma-Aldrich, P8340]). After sonication, cell lysates were centrifuged at 14,000 ×g for 20 min at 4°C and the supernatants were collected for further analysis. Lysates were mixed with 2x or 5x protein sample buffer and boiled at 100°C for 5 min. For ATG9A protein, lysates were not subjected to boiling to prevent protein aggregation caused by the transmembrane nature of ATG9A. Samples were separated on Tris-glycine gels (6–12%) and transferred to 0.45 μm PVDF membranes (Merck, ipvh00010). Membranes were blocked with 5% skim milk diluted in TBS-T (20 mM Tris-HCl, pH 7.4, 137 mM NaCl, 0.1% Tween-20 [Sigma-Aldrich, P1379]) for 30 min and incubated with respective primary antibodies overnight at 4°C. After three TBS-T washes, membranes were incubated with horseradish peroxidase (HRP)-conjugated secondary

antibodies for 45 min at RT. The chemiluminescence signals were developed using an enhanced chemiluminescence reagent (AbClon, ABC-3001) and detected with Amersham Imager 680 (GE Healthcare, Chicago, IL). For immunoprecipitation, the same amounts of protein (500–1000 μg) were incubated with primary antibodies overnight at 4°C, followed by incubation with Protein A-Sepharose beads (GE Healthcare 17,528,001) or Pierce Protein A/G Magnetic beads (Thermo Scientific 88,803) for 2 h at 4°C. Beads were washed three times with lysis buffer, eluted with 2 × protein sample buffer (100 mM Tris-HCl, pH 6.8, 4% SDS, 20% glycerol, 0.2% bromophenol blue, 2% β-mercaptoethanol), and boiled at 100°C for 5 min. The following procedures were carried out according to the western blotting protocol.

Adeno-associated virus (AAV) production

HEK-293T cells were triply transfected with an inverted terminal repeat (ITR) vector containing the gene of interest, pAAV-DJ and pHelper (Cell Biolabs) in a 1:1:1 molecular weight ratio. The transfection was performed using PEI and the cells were harvested 48–72 h after transfection. Cell pellets were resuspended in phosphate-buffered saline (PBS) and subjected to four rounds of freezing and melting with a cooling and warming bath. The AAVs were purified using polyethylene glycol 8000 (PEG 8000)-NaCl and extracted with chloroform to remove hydrophilic proteins and PEG residues. After 30 min of incubation to remove chloroform, the collected AAVs were concentrated using dialysis tubes and stored at –80°C. Genomic titers of AAV were determined using the StepOne Real-Time PCR System (Applied Biosystems, Waltham, MA), and 10 multiplicities of infection (MOI) of AAV were used for infection.

Fluorescence imaging

Neurons at DIV 14–16 were imaged in Tyrode's solution either using a Nikon spinning disk confocal microscope (inverted Nikon Ti microscope equipped with a CSU-X1 spinning disk confocal) equipped with a 40x oil-immersion objective lens (Plan Apo NA 1.30) and a Neo sCMOS camera (Andor Technology, Belfast, Northern Ireland) driven by NIS-Elements software (Nikon, Tokyo, Japan), using a confocal laser scanning microscope FV3000 (Olympus, Tokyo, Japan) equipped with a 60x oil-immersion objective lens (UPlanSApo NA 1.42), or using a ZEISS laser scanning microscope LSM980 (Carl Zeiss, Oberkochen, Germany) equipped with a 63x oil-immersion objective lens (Plan-Apochromat 1.4) and an AxioCam305 mono camera driven by Zen blue 3.4 software. Super-resolution images were acquired on a Zeiss LSM980 microscope equipped with a 32 circularly arranged Airyscan2 area detector and a 63x oil-immersion objective lens (Plan-Apochromat 1.4) with a zoom factor of 2.4 × 2.4 and frame size of 56.12 × 56.12 μm. Images were further enhanced using the Joint deconvolution (jDCV) algorithm in Zen blue (theoretical resolution limit: 120 nm lateral, 350 nm axial). To analyze protein colocalization, Mander's colocalization coefficients (MCCs) were calculated with ImageJ (NIH) and the JACoP plugin (<https://imagej.nih.gov/ij/plugins/jacop.html>).

gins/track/jacop2.html). All values are presented as the mean \pm SEM. The average MCC value of each sample was compared using either a Student's *t*-test or a one-way ANOVA followed by Tukey's post hoc test. The significance of all data is reported as * p < 0.05, ** p < 0.01, *** p < 0.001.

For mFT-SV2 fluorescence imaging, neurons were co-transfected at DIV 11 with 2 μ g of scRNA or shRNA-*Scamp5* and 6 μ g FU-mFT-SV2, followed by imaging 48 h post-transfection. To prevent light-induced chromophore maturation, as FTs can undergo photoconversion from blue to red under high-intensity violet light, images were captured sequentially – first in the red channel, then in the blue channel. The blue/red fluorescence intensities in boutons were quantified after subtracting background autofluorescence measured from corresponding regions of non-fluorescent cells on the same coverslip. The red:blue ratio heatmap was generated using a custom MATLAB script to visualize relative intensity differences between the red and blue channels, enabling precise quantification and spatial mapping of color intensity variations within the analyzed images.

Cycloheximide chase assay

Primary rat cortical neurons at DIV 13 were treated with 0.2 μ g/ μ l cycloheximide (CHX; Sigma-Aldrich, C7698) or an equivalent amount of DMSO for 24 h. For combined proteasome inhibition, 10 μ M MG132 (AG Scientific, M-1157) was added together with CHX for either 24 or 48 h. All treatments were performed on both control and AAV-mediated SCAMP5 knockdown neurons. Following treatment, cells were lysed directly in 2x protein sample buffer containing 1 mM PMSF and 1x protease inhibitor cocktail, then centrifuged at 14,000 \times g for 1 h at 4°C. Supernatants were collected and analyzed by western blotting. Samples were separated on Tris-glycine gels (15%) and transferred to 0.2 μ m nitrocellulose membranes (Thermo Fisher Scientific 77,012).

Statistical analysis

All experimental data are presented as mean \pm standard error of the mean (SEM). For each experiment, the number of independent experiments (*n*) and total number of analyzed cells, boutons, or axons are indicated in the figure legends. Each independent experiment consisted of analyzing 3–5 neurons unless otherwise specified. Statistical analyses were performed using appropriate tests based on the experimental design and data distribution. For comparisons between two groups, unpaired Student's *t*-tests were used. For multiple group comparisons, one-way analysis of variance (ANOVA) followed by Tukey's honestly significant difference (HSD) post hoc test was employed to determine specific differences between groups. Statistical significance was defined as follows: * p < 0.05, ** p < 0.01, *** p < 0.001. Non-significant results are indicated as "ns" where p \geq 0.05. All statistical analyses were performed using GraphPad Prism software (GraphPad, Boston, MA) and p-values are reported to three decimal places where applicable.

Acknowledgements

Molecular graphics and analyses performed with UCSF ChimeraX, developed by the Resource for Biocomputing, Visualization, and Informatics at the University of California, San Francisco, with support from National Institutes of Health R01-GM129325 and the Office of Cyber Infrastructure and Computational Biology, National Institute of Allergy and Infectious Diseases (<https://www.cgl.ucsf.edu/chimerax/docs/credits.html>). Schematic illustrations in Figures 8E and 9 were created by <https://www.biorender.com>.

S.H.R., J.L., S.-E.L., S.C. performed conceptualization. S.H.R., J.L., U.L., K.K., G.J., J.O. and S.-E.L. performed the research. S.H.R., S.-E.L. and S.C. wrote the original draft.

Author contributions

CRedit: **Seung Hyun Ryu:** Conceptualization, Data curation, Formal analysis, Investigation, Writing – original draft; **Jungmihn Lee:** Data curation, Formal analysis, Investigation, Writing – original draft; **Unghwi Lee:** Formal analysis, Investigation; **Kitae Kim:** Formal analysis, Investigation; **Go-Eun Jun:** Investigation; **Jeongmin Oh:** Formal analysis, Investigation; **Sang-Eun Lee:** Conceptualization, Data curation, Formal analysis, Investigation, Writing – original draft; **Sunghoe Chang:** Conceptualization, Formal analysis, Funding acquisition, Supervision, Validation, Writing – original draft.

Funding

This research was supported in part by grants from the National Research Foundation of Korea [RS-2022-NR070478, RS-2024-00437688, and RS-2024-00402116] to S.C., and the Industry-Academic Cooperation Foundation fund, CHA University [Project No. CHA-202500420001] to S.-E.L.

Disclosure statement

No potential conflict of interest was reported by the author(s).

Data availability statement

The datasets used and/or analyzed during the current study are available from the corresponding author on reasonable request.

ORCID

Sunghoe Chang  <http://orcid.org/0000-0002-3446-7288>

References

- [1] Martinez-Vicente M, Cuervo AM. Autophagy and neurodegeneration: when the cleaning crew goes on strike. *Lancet Neurol*. 2007;6(4):352–361. doi: [10.1016/S1474-4422\(07\)70076-5](https://doi.org/10.1016/S1474-4422(07)70076-5)
- [2] Mizushima N, Levine B, Cuervo AM, et al. Autophagy fights disease through cellular self-digestion. *Nature*. 2008;451(7182):1069–1075. doi: [10.1038/nature06639](https://doi.org/10.1038/nature06639)
- [3] Korolchuk VI, Rubinsztein DC. Regulation of autophagy by lysosomal positioning. *Autophagy*. 2011;7(8):927–928. doi: [10.4161/auto.7.8.15862](https://doi.org/10.4161/auto.7.8.15862)
- [4] Sumitomo A, Tomoda T. Autophagy in neuronal physiology and disease. *Curr Opin Pharmacol*. 2021;60:133–140. doi: [10.1016/j.coph.2021.07.013](https://doi.org/10.1016/j.coph.2021.07.013)
- [5] Nakatogawa H. Mechanisms governing autophagosome biogenesis. *Nat Rev Mol Cell Biol*. 2020;21(8):439–458. doi: [10.1038/s41580-020-0241-0](https://doi.org/10.1038/s41580-020-0241-0)

- [6] Lee JA. Neuronal autophagy: a housekeeper or a fighter in neuronal cell survival? *Exp Neurobiol.* **2012**;21(1):1–8. doi: [10.5607/en.2012.21.1.1](https://doi.org/10.5607/en.2012.21.1.1)
- [7] Wong YC, Holzbaur EL. Autophagosome dynamics in neurodegeneration at a glance. *J Cell Sci.* **2015**;128(7):1259–1267. doi: [10.1242/jcs.161216](https://doi.org/10.1242/jcs.161216)
- [8] Xilouri M, Stefanis L. Autophagy in the central nervous system: implications for neurodegenerative disorders. *CNS Neurol Disord Drug Targets.* **2010**;9(6):701–719. doi: [10.2174/187152710793237421](https://doi.org/10.2174/187152710793237421)
- [9] Boehm M, Aguilar RC, Bonifacino JS. Functional and physical interactions of the adaptor protein complex AP-4 with ADP-ribosylation factors (ARFs). *Embo J.* **2001**;20(22):6265–6276. doi: [10.1093/emboj/20.22.6265](https://doi.org/10.1093/emboj/20.22.6265)
- [10] Highland CM, Fromme JC, Glick B. Arf1 directly recruits the Pik1-Frq1 PI4K complex to regulate the final stages of Golgi maturation. *Mol Biol Cell.* **2021**;32(10):1064–1080. doi: [10.1091/mbc.E21-02-0069](https://doi.org/10.1091/mbc.E21-02-0069)
- [11] Ito Y, Esnay N, Platre MP, et al. Sphingolipids mediate polar sorting of PIN2 through phosphoinositide consumption at the trans-Golgi network. *Nat Commun.* **2021**;12(1):4267. doi: [10.1038/s41467-021-24548-0](https://doi.org/10.1038/s41467-021-24548-0)
- [12] Kutchukian C, Vivas O, Casas M, et al. Npc1 regulates the distribution of phosphatidylinositol 4-kinases at Golgi and lysosomal membranes. *Embo J.* **2021**;40(13):e105990. doi: [10.1525/embj.2020105990](https://doi.org/10.1525/embj.2020105990)
- [13] Burgos PV, Mardones GA, Rojas AL, et al. Sorting of the Alzheimer's disease amyloid precursor protein mediated by the AP-4 complex. *Dev Cell.* **2010**;18(3):425–436. doi: [10.1016/j.devcel.2010.01.015](https://doi.org/10.1016/j.devcel.2010.01.015)
- [14] Tan JZA, Gleeson PA. The trans-Golgi network is a major site for alpha-secretase processing of amyloid precursor protein in primary neurons. *J Biol Chem.* **2019**;294(5):1618–1631. doi: [10.1074/jbc.RA118.005222](https://doi.org/10.1074/jbc.RA118.005222)
- [15] Raza MH, Mattera R, Morell R, et al. Association between rare variants in AP4E1, a component of intracellular trafficking, and persistent stuttering. *Am J Hum Genet.* **2015**;97(5):715–725. doi: [10.1016/j.ajhg.2015.10.007](https://doi.org/10.1016/j.ajhg.2015.10.007)
- [16] Mattera R, Park SY, De Pace R, et al. Ap-4 mediates export of ATG9A from the trans-Golgi network to promote autophagosome formation. *Proc Natl Acad Sci USA.* **2017**;114(50):E10697–E10706. doi: [10.1073/pnas.1717327114](https://doi.org/10.1073/pnas.1717327114)
- [17] Davies AK, Itzhak DN, Edgar JR, et al. Ap-4 vesicles contribute to spatial control of autophagy via RUSC-dependent peripheral delivery of ATG9A. *Nat Commun.* **2018**;9(1):3958. doi: [10.1038/s41467-018-06172-7](https://doi.org/10.1038/s41467-018-06172-7)
- [18] Folsch H, Ohno H, Bonifacino JS, et al. A novel clathrin adaptor complex mediates basolateral targeting in polarized epithelial cells. *Cell.* **1999**;99(2):189–198. doi: [10.1016/S0092-8674\(00\)81650-5](https://doi.org/10.1016/S0092-8674(00)81650-5)
- [19] Simmen T, Höning S, Icking A, et al. Ap-4 binds basolateral signals and participates in basolateral sorting in epithelial MDCK cells. *Nat Cell Biol.* **2002**;4(2):154–159. doi: [10.1038/ncb745](https://doi.org/10.1038/ncb745)
- [20] Yap CC, Murate M, Kishigami S, et al. Adaptor protein complex-4 (AP-4) is expressed in the central nervous system neurons and interacts with glutamate receptor delta2. *Mol Cell Neurosci.* **2003**;24(2):283–295. doi: [10.1016/S1044-7431\(03\)00164-7](https://doi.org/10.1016/S1044-7431(03)00164-7)
- [21] Matsuda S, Miura E, Matsuda K, et al. Accumulation of AMPA receptors in autophagosomes in neuronal axons lacking adaptor protein AP-4. *Neuron.* **2008**;57(5):730–745. doi: [10.1016/j.neuron.2008.02.012](https://doi.org/10.1016/j.neuron.2008.02.012)
- [22] Craige B, Salazar G, Faundez V, et al. Phosphatidylinositol-4-kinase type II alpha contains an AP-3-sorting motif and a kinase domain that are both required for endosome traffic. *Mol Biol Cell.* **2008**;19(4):1415–1426. doi: [10.1091/mbc.e07-12-1239](https://doi.org/10.1091/mbc.e07-12-1239)
- [23] Hausser A, Storz P, Märkens S, et al. Protein kinase D regulates vesicular transport by phosphorylating and activating phosphatidylinositol-4 kinase IIIbeta at the Golgi complex. *Nat Cell Biol.* **2005**;7(9):880–886. doi: [10.1038/ncb1289](https://doi.org/10.1038/ncb1289)
- [24] Haynes LP, Thomas GM, Burgoyne RD. Interaction of neuronal calcium sensor-1 and ADP-ribosylation factor 1 allows bidirectional control of phosphatidylinositol 4-kinase beta and trans-Golgi network-plasma membrane traffic. *J Biol Chem.* **2005**;280(7):6047–6054. doi: [10.1074/jbc.M413090200](https://doi.org/10.1074/jbc.M413090200)
- [25] Stalder D, Yakunin I, Pereira C, et al. Recruitment of PI4KIIIbeta to the Golgi by ACBD3 is dependent on an upstream pathway of a SNARE complex and golgins. *Mol Biol Cell.* **2024**;35(2):ar20. doi: [10.1091/mbc.E23-09-0376](https://doi.org/10.1091/mbc.E23-09-0376)
- [26] Daboussi L, Costaguta G, Ghukasyan R, et al. Conserved role for GGA proteins in phosphatidylinositol 4-kinase localization to the trans-Golgi network. *Proc Natl Acad Sci USA.* **2017**;114(13):3433–3438. doi: [10.1073/pnas.1615163114](https://doi.org/10.1073/pnas.1615163114)
- [27] Maday S, Holzbaur EL. Autophagosome biogenesis in primary neurons follows an ordered and spatially regulated pathway. *Dev Cell.* **2014**;30(1):71–85. doi: [10.1016/j.devcel.2014.06.001](https://doi.org/10.1016/j.devcel.2014.06.001)
- [28] Yue Z. Regulation of neuronal autophagy in axon: implication of autophagy in axonal function and dysfunction/degeneration. *Autophagy.* **2007**;3(2):139–141. doi: [10.4161/auto.3602](https://doi.org/10.4161/auto.3602)
- [29] Stavoe AK, Kargbo-Hill S, Hall D, et al. KIF1A/UNC-104 transports ATG-9 to regulate neurodevelopment and autophagy at synapses. *Dev Cell.* **2016**;38(2):171–185. doi: [10.1016/j.devcel.2016.06.012](https://doi.org/10.1016/j.devcel.2016.06.012)
- [30] Crawley O, Opperman KJ, Desbois M, et al. Autophagy is inhibited by ubiquitin ligase activity in the nervous system. *Nat Commun.* **2019**;10(1):5017. doi: [10.1038/s41467-019-12804-3](https://doi.org/10.1038/s41467-019-12804-3)
- [31] Xuan Z, Yang S, Clark B, et al. The active zone protein clarinet regulates synaptic sorting of ATG-9 and presynaptic autophagy. *PLOS Biol.* **2023**;21(4):e3002030. doi: [10.1371/journal.pbio.3002030](https://doi.org/10.1371/journal.pbio.3002030)
- [32] Soukup SF, Kuenen S, Vanhauwaert R, et al. A LRRK2-dependent EndophilinA phosphoswitch is critical for macroautophagy at presynaptic terminals. *Neuron.* **2016**;92(4):829–844. doi: [10.1016/j.neuron.2016.09.037](https://doi.org/10.1016/j.neuron.2016.09.037)
- [33] Okerlund ND, Schneider K, Leal-Ortiz S, et al. Bassoon controls presynaptic autophagy through Atg5. *Neuron.* **2017**;93(4):897–913 e7. doi: [10.1016/j.neuron.2017.01.026](https://doi.org/10.1016/j.neuron.2017.01.026)
- [34] Vanhauwaert R, Kuenen S, Masius R, et al. The SAC1 domain in synaptotagmin is required for autophagosome maturation at presynaptic terminals. *Embo J.* **2017**;36(10):1392–1411. doi: [10.1525/embj.201695773](https://doi.org/10.1525/embj.201695773)
- [35] Hirst J, Irving C, Borner GH. Adaptor protein complexes AP-4 and AP-5: new players in endosomal trafficking and progressive spastic paraplegia. *Traffic.* **2013**;14(2):153–164. doi: [10.1111/tra.12028](https://doi.org/10.1111/tra.12028)
- [36] Abou Jamra R, Philippe O, Raas-Rothschild A, et al. Adaptor protein complex 4 deficiency causes severe autosomal-recessive intellectual disability, progressive spastic paraplegia, shy character, and short stature. *Am J Hum Genet.* **2011**;88(6):788–795. doi: [10.1016/j.ajhg.2011.04.019](https://doi.org/10.1016/j.ajhg.2011.04.019)
- [37] Moreno-De-Luca A, Helmers SL, Mao H, et al. Adaptor protein complex-4 (AP-4) deficiency causes a novel autosomal recessive cerebral palsy syndrome with microcephaly and intellectual disability. *J Med Genet.* **2011**;48(2):141–144. doi: [10.1136/jmg.2010.082263](https://doi.org/10.1136/jmg.2010.082263)
- [38] Ebrahimi-Fakhari D, Cheng C, Dies K, et al. Clinical and genetic characterization of APB1-associated SPG47. *Am J Med Genet Pt A.* **2018**;176(2):311–318. doi: [10.1002/ajmg.a.38561](https://doi.org/10.1002/ajmg.a.38561)
- [39] Ivankovic D, Drew J, Lesept F, et al. Axonal autophagosome maturation defect through failure of ATG9A sorting underpins pathology in AP-4 deficiency syndrome. *Autophagy.* **2020**;16(3):391–407. doi: [10.1080/15548627.2019.1615302](https://doi.org/10.1080/15548627.2019.1615302)
- [40] Yang S, Park D, Manning L, et al. Presynaptic autophagy is coupled to the synaptic vesicle cycle via ATG-9. *Neuron.* **2022**;110(5):824–840. e10. doi: [10.1016/j.neuron.2021.12.031](https://doi.org/10.1016/j.neuron.2021.12.031)
- [41] Jahne S, Mikulasch F, Heuer HGH, et al. Presynaptic activity and protein turnover are correlated at the single-synapse level. *Cell Rep.* **2021**;34(11):108841. doi: [10.1016/j.celrep.2021.108841](https://doi.org/10.1016/j.celrep.2021.108841)

- [42] Imai K, Hao F, Fujita N, et al. Atg9a trafficking through the recycling endosomes is required for autophagosome formation. *J Cell Sci.* **2016**;129(20):3781–3791. doi: [10.1242/jcs.196196](https://doi.org/10.1242/jcs.196196)
- [43] Guardia CM, Tan X-F, Lian T, et al. Structure of human ATG9A, the only transmembrane protein of the core autophagy machinery. *Cell Rep.* **2020**;31(13):107837. doi: [10.1016/j.celrep.2020.107837](https://doi.org/10.1016/j.celrep.2020.107837)
- [44] Fernandez-Chacon R, Sudhof TC. Novel SCAMPs lacking NPF repeats: ubiquitous and synaptic vesicle-specific forms implicate SCAMPs in multiple membrane-trafficking functions. *J Neurosci.* **2000**;20(21):7941–7950. doi: [10.1523/JNEUROSCI.20-21-07941.2000](https://doi.org/10.1523/JNEUROSCI.20-21-07941.2000)
- [45] Castle A, Castle D. Ubiquitously expressed secretory carrier membrane proteins (SCAMPs) 1–4 mark different pathways and exhibit limited constitutive trafficking to and from the cell surface. *J Cell Sci.* **2005**;118(Pt 16):3769–3780. doi: [10.1242/jcs.02503](https://doi.org/10.1242/jcs.02503)
- [46] Hubert L, Cannata Serio M, Villoing-Gaudé L, et al. De novo SCAMP5 mutation causes a neurodevelopmental disorder with autistic features and seizures. *J Med Genet.* **2020**;57(2):138–144. doi: [10.1136/jmedgenet-2018-105927](https://doi.org/10.1136/jmedgenet-2018-105927)
- [47] Zhang D, Yuan C, Liu M, et al. Deficiency of SCAMP5 leads to pediatric epilepsy and dysregulation of neurotransmitter release in the brain. *Hum Genet.* **2020**;139(4):545–555. doi: [10.1007/s00439-020-02123-9](https://doi.org/10.1007/s00439-020-02123-9)
- [48] Jiao X, Morleo M, Nigro V, et al. Identification of an identical de novo SCAMP5 missense variant in four unrelated patients with seizures and severe neurodevelopmental delay. *Front Pharmacol.* **2020**;11:599191. doi: [10.3389/fphar.2020.599191](https://doi.org/10.3389/fphar.2020.599191)
- [49] Zhao H, Kim Y, Park J, et al. Scamp5 plays a critical role in synaptic vesicle endocytosis during high neuronal activity. *J Neurosci.* **2014**;34(30):10085–10095. doi: [10.1523/JNEUROSCI.2156-14.2014](https://doi.org/10.1523/JNEUROSCI.2156-14.2014)
- [50] Park D, Lee U, Cho E, et al. Impairment of release site clearance within the active zone by reduced SCAMP5 expression causes short-term depression of synaptic release. *Cell Rep.* **2018**;22(12):3339–3350. doi: [10.1016/j.celrep.2018.02.088](https://doi.org/10.1016/j.celrep.2018.02.088)
- [51] Lee U, Choi C, Ryu SH, et al. Scamp5 plays a critical role in axonal trafficking and synaptic localization of NHE6 to adjust quantal size at glutamatergic synapses. *Proc Natl Acad Sci USA.* **2021**;118(2):e2011371118. doi: [10.1073/pnas.2011371118](https://doi.org/10.1073/pnas.2011371118)
- [52] Fernandez-Chacon R, Achiriloae M, Janz R, et al. Scamp1 function in endocytosis. *J Biol Chem.* **2000**;275(17):12752–12756. doi: [10.1074/jbc.275.17.12752](https://doi.org/10.1074/jbc.275.17.12752)
- [53] Liu L, Guo Z, Tieu Q, et al. Role of secretory carrier membrane protein SCAMP2 in granule exocytosis. *Mol Biol Cell.* **2002**;13(12):4266–4278. doi: [10.1091/mbc.e02-03-0136](https://doi.org/10.1091/mbc.e02-03-0136)
- [54] Singleton D, Wu T, Castle J. Three mammalian SCAMPs (secretory carrier membrane proteins) are highly related products of distinct genes having similar subcellular distributions. *J Cell Sci.* **1997**;110(17):2099–2107. doi: [10.1242/jcs.110.17.2099](https://doi.org/10.1242/jcs.110.17.2099)
- [55] Thomas P, Wohlford D, Aoh QL. Scamp 3 is a novel regulator of endosomal morphology and composition. *Biochem Biophys Res Commun.* **2016**;478(3):1028–1034. doi: [10.1016/j.bbrc.2016.08.012](https://doi.org/10.1016/j.bbrc.2016.08.012)
- [56] Lee U, Ryu SH, Chang S. Scamp5 mediates activity-dependent enhancement of NHE6 recruitment to synaptic vesicles during synaptic plasticity. *Mol Brain.* **2021**;14(1):47. doi: [10.1186/s13041-021-00763-0](https://doi.org/10.1186/s13041-021-00763-0)
- [57] Noh JY, Lee H, Song S, et al. Scamp5 links endoplasmic reticulum stress to the accumulation of expanded polyglutamine protein aggregates via endocytosis inhibition. *J Biol Chem.* **2009**;284(17):11318–11325.
- [58] Yang Y, Qin M, Bao P, et al. Secretory carrier membrane protein 5 is an autophagy inhibitor that promotes the secretion of alpha-synuclein via exosome. *PLOS ONE.* **2017**;12(7):e0180892. doi: [10.1371/journal.pone.0180892](https://doi.org/10.1371/journal.pone.0180892)
- [59] Hoffmann S, Orlando M, Andrzejak E, et al. Light-activated ROS production induces synaptic autophagy. *J Neurosci.* **2019**;39(12):2163–2183. doi: [10.1523/JNEUROSCI.1317-18.2019](https://doi.org/10.1523/JNEUROSCI.1317-18.2019)
- [60] Shehata M, Matsumura H, Okubo-Suzuki R, et al. Neuronal stimulation induces autophagy in hippocampal neurons that is involved in AMPA receptor degradation after chemical long-term depression. *J Neurosci.* **2012**;32(30):10413–10422. doi: [10.1523/JNEUROSCI.4533-11.2012](https://doi.org/10.1523/JNEUROSCI.4533-11.2012)
- [61] De Pace R, Skirzewski M, Damme M, et al. Altered distribution of ATG9A and accumulation of axonal aggregates in neurons from a mouse model of AP-4 deficiency syndrome. *PLOS Genet.* **2018**;14(4):e1007363. doi: [10.1371/journal.pgen.1007363](https://doi.org/10.1371/journal.pgen.1007363)
- [62] Wang YJ, Wang J, Sun HQ, et al. Phosphatidylinositol 4 phosphate regulates targeting of clathrin adaptor AP-1 complexes to the Golgi. *Cell.* **2003**;114(3):299–310. doi: [10.1016/S0092-8674\(03\)00603-2](https://doi.org/10.1016/S0092-8674(03)00603-2)
- [63] Daboussi L, Costaguta G, Payne GS. Phosphoinositide-mediated clathrin adaptor progression at the trans-Golgi network. *Nat Cell Biol.* **2012**;14(3):239–248. doi: [10.1038/ncb2427](https://doi.org/10.1038/ncb2427)
- [64] Klima M, Tóth DJ, Hexnerova R, et al. Structural insights and in vitro reconstitution of membrane targeting and activation of human PI4KB by the ACBD3 protein. *Sci Rep.* **2016**;6(1):23641. doi: [10.1038/srep23641](https://doi.org/10.1038/srep23641)
- [65] Jun YW, Lee JA, Jang DJ. Novel GFP-fused protein probes for detecting phosphatidylinositol-4-phosphate in the plasma membrane. *Anim Cells Syst (Seoul).* **2019**;23(3):164–169. doi: [10.1080/19768354.2019.1599424](https://doi.org/10.1080/19768354.2019.1599424)
- [66] Ivanova D, Cousin MA. Synaptic vesicle recycling and the endolysosomal system: a reappraisal of form and function. *Front Synaptic Neurosci.* **2022**;14. doi: [10.3389/fnsyn.2022.826098](https://doi.org/10.3389/fnsyn.2022.826098)
- [67] Hoffmann-Conaway S, Brockmann MM, Schneider K, et al. Parkin contributes to synaptic vesicle autophagy in bassoon-deficient mice. *Elife.* **2020**;9:e56590. doi: [10.7554/eLife.56590](https://doi.org/10.7554/eLife.56590)
- [68] Subach FV, Subach OM, Gundorov IS, et al. Monomeric fluorescent timers that change color from blue to red report on cellular trafficking. *Nat Chem Biol.* **2009**;5(2):118–126. doi: [10.1038/nchembio.138](https://doi.org/10.1038/nchembio.138)
- [69] Lieberman OJ, Sulzer D. The synaptic autophagy cycle. *J Mol Biol.* **2020**;432(8):2589–2604. doi: [10.1016/j.jmb.2019.12.028](https://doi.org/10.1016/j.jmb.2019.12.028)
- [70] Bademosi AT, Decet M, Kuenen S, et al. EndophilinA-dependent coupling between activity-induced calcium influx and synaptic autophagy is disrupted by a Parkinson-risk mutation. *Neuron.* **2023**;111(9):1402–1422 e13. doi: [10.1016/j.neuron.2023.02.001](https://doi.org/10.1016/j.neuron.2023.02.001)
- [71] Hamamoto K, Liang X, Ito A, et al. Unveiling the physiological impact of ESCRT-dependent autophagosome closure by targeting the VPS37A ubiquitin E2 variant-like domain. *Cell Rep.* **2024**;43(12):115016. doi: [10.1016/j.celrep.2024.115016](https://doi.org/10.1016/j.celrep.2024.115016)
- [72] Law AH, Chow CM, Jiang L. Secretory carrier membrane proteins. *Protoplasma.* **2012**;249(2):269–283. doi: [10.1007/s00709-011-0295-0](https://doi.org/10.1007/s00709-011-0295-0)
- [73] Park D, Wu Y, Wang X, et al. Synaptic vesicle proteins and ATG9A self-organize in distinct vesicle phases within synapsin condensates. *Nat Commun.* **2023**;14(1):455. doi: [10.1038/s41467-023-36081-3](https://doi.org/10.1038/s41467-023-36081-3)
- [74] Castermans D, Volders K, Crepel A, et al. Scamp5, NBEA and AMISYN: three candidate genes for autism involved in secretion of large dense-core vesicles. *Hum Mol Genet.* **2010**;19(7):1368–1378. doi: [10.1093/hmg/ddq013](https://doi.org/10.1093/hmg/ddq013)
- [75] Binotti B, Ninov M, Cepeda AP, et al. Atg9 resides on a unique population of small vesicles in presynaptic nerve terminals. *Autophagy.* **2024**;20(4):883–901. doi: [10.1080/15548627.2023.2274204](https://doi.org/10.1080/15548627.2023.2274204)
- [76] Uddin MS, Stachowiak A, Mamun AA, et al. Autophagy and Alzheimer's disease: from molecular mechanisms to therapeutic implications. *Front Aging Neurosci.* **2018**;10:04. doi: [10.3389/fnagi.2018.00004](https://doi.org/10.3389/fnagi.2018.00004)

- [77] Ali NH, Al-Kuraishi HM, Al-Gareeb AI, et al. Autophagy and autophagy signaling in epilepsy: possible role of autophagy activator. *Mol Med*. **2023**;29(1):142. doi: [10.1186/s10020-023-00742-2](https://doi.org/10.1186/s10020-023-00742-2)
- [78] Deng Z, Zhou X, Lu J-H, et al. Autophagy deficiency in neurodevelopmental disorders. *Cell Biosci*. **2021**;11(1):214. doi: [10.1186/s13578-021-00726-x](https://doi.org/10.1186/s13578-021-00726-x)
- [79] Nguyen TN, Padman BS, Lazarou M. Deciphering the molecular signals of PINK1/Parkin mitophagy. *Trends Cell Biol*. **2016**;26(10):733–744. doi: [10.1016/j.tcb.2016.05.008](https://doi.org/10.1016/j.tcb.2016.05.008)
- [80] Zapata-Munoz J, Villarejo-Zori B, Largo-Barrientos P, et al. Towards a better understanding of the neuro-developmental role of autophagy in sickness and in health. *Cell Stress*. **2021**;5(7):99–118. doi: [10.15698/cst2021.07.253](https://doi.org/10.15698/cst2021.07.253)
- [81] Labuhn M, Adams FF, Ng M, et al. Refined sgRNA efficacy prediction improves large- and small-scale CRISPR-Cas9 applications. *Nucleic Acids Res*. **2018**;46(3):1375–1385. doi: [10.1093/nar/gkx1268](https://doi.org/10.1093/nar/gkx1268)
- [82] Stemmer M, Thumberger T, Del Sol Keyer M, et al. Cctop: an intuitive, flexible and reliable CRISPR/Cas9 target prediction tool. *PLOS ONE*. **2015**;10(4):e0124633. doi: [10.1371/journal.pone.0124633](https://doi.org/10.1371/journal.pone.0124633)
- [83] Cong L, Ran FA, Cox D, et al. Multiplex genome engineering using CRISPR/Cas systems. *Science*. **2013**;339(6121):819–823. doi: [10.1126/science.1231143](https://doi.org/10.1126/science.1231143)
- [84] Hsu PD, Scott DA, Weinstein JA, et al. DNA targeting specificity of RNA-guided Cas9 nucleases. *Nat Biotechnol*. **2013**;31(9):827–832. doi: [10.1038/nbt.2647](https://doi.org/10.1038/nbt.2647)
- [85] Ran FA, Hsu P, Lin C-Y, et al. Double nicking by RNA-guided CRISPR Cas9 for enhanced genome editing specificity. *Cell*. **2013**;154(6):1380–1389. doi: [10.1016/j.cell.2013.08.021](https://doi.org/10.1016/j.cell.2013.08.021)
- [86] Ran FA, Hsu PD, Wright J, et al. Genome engineering using the CRISPR-Cas9 system. *Nat protoc*. **2013**;8(11):2281–2308. doi: [10.1038/nprot.2013.143](https://doi.org/10.1038/nprot.2013.143)
- [87] Lee SE, Kim Y, Han J-K, et al. NArgBP2 regulates excitatory synapse formation by controlling dendritic spine morphology. *Proc Natl Acad Sci USA*. **2016**;113(24):6749–6754. doi: [10.1073/pnas.1600944113](https://doi.org/10.1073/pnas.1600944113)
- [88] Goddard TD, Huang CC, Meng EC, et al. UCSF chimeraX: meeting modern challenges in visualization and analysis. *Protein Sci*. **2018**;27(1):14–25. doi: [10.1002/pro.3235](https://doi.org/10.1002/pro.3235)
- [89] Meng EC, Goddard TD, Pettersen EF, et al. Ucsf ChimeraX: tools for structure building and analysis. *Protein Sci*. **2023**;32(11):e4792. doi: [10.1002/pro.4792](https://doi.org/10.1002/pro.4792)
- [90] Pettersen EF, Goddard TD, Huang CC, et al. UCSF ChimeraX: structure visualization for researchers, educators, and developers. *Protein Sci*. **2021**;30(1):70–82. doi: [10.1002/pro.3943](https://doi.org/10.1002/pro.3943)
- [91] Jumper J, Evans R, Pritzel A, et al. Highly accurate protein structure prediction with AlphaFold. *Nature*. **2021**;596(7873):583–589. doi: [10.1038/s41586-021-03819-2](https://doi.org/10.1038/s41586-021-03819-2)
- [92] Varadi M, Bertoni D, Magana P, et al. Alphafold protein structure database in 2024: providing structure coverage for over 214 million protein sequences. *Nucleic Acids Res*. **2024**;52(D1):D368–D375. doi: [10.1093/nar/gkad1011](https://doi.org/10.1093/nar/gkad1011)